

NBER WORKING PAPER SERIES

SOLAR GEOENGINEERING, LEARNING, AND EXPERIMENTATION

David L. Kelly  
Garth Heutel  
Juan B. Moreno-Cruz  
Soheil Shayegh

Working Paper 28442  
<http://www.nber.org/papers/w28442>

NATIONAL BUREAU OF ECONOMIC RESEARCH  
1050 Massachusetts Avenue  
Cambridge, MA 02138  
February 2021

We thank David Anthoff and conference and seminar participants at the AERE summer conference, the University of California at Berkeley, the SEA annual conference, the WCERE, and the 17th Occasional Workshop on Environmental and Resource Economics for valuable comments. The views expressed herein are those of the authors and do not necessarily reflect the views of the National Bureau of Economic Research.

NBER working papers are circulated for discussion and comment purposes. They have not been peer-reviewed or been subject to the review by the NBER Board of Directors that accompanies official NBER publications.

© 2021 by David L. Kelly, Garth Heutel, Juan B. Moreno-Cruz, and Soheil Shayegh. All rights reserved. Short sections of text, not to exceed two paragraphs, may be quoted without explicit permission provided that full credit, including © notice, is given to the source.

Solar Geoengineering, Learning, and Experimentation  
David L. Kelly, Garth Heutel, Juan B. Moreno-Cruz, and Soheil Shayegh  
NBER Working Paper No. 28442  
February 2021  
JEL No. D83,Q54

### **ABSTRACT**

Solar geoengineering (SGE) can combat climate change by directly reducing temperatures. Both SGE and the climate itself are surrounded by great uncertainties. Implementing SGE affects learning about these uncertainties. We model endogenous learning over two uncertainties: the sensitivity of temperatures to carbon concentrations (the climate sensitivity), and the effectiveness of SGE in lowering temperatures. We present both theoretical and simulation results from an integrated assessment model, focusing on the informational value of SGE experimentation. Surprisingly, under current calibrated conditions, SGE deployment slows learning, causing a less informed decision. For any reasonably sized experimental SGE deployment, the temperature change becomes closer to zero, and thus more obscured by noisy weather shocks. Still, some SGE use is optimal despite, not because of, its informational value. The optimal amount of SGE is very sensitive to beliefs about both uncertainties.

David L. Kelly  
Department of Economics  
University of Miami  
Box 248126  
Coral Gables, FL 33146  
dkelly@miami.edu

Garth Heutel  
436 Andrew Young School  
Department of Economics  
Georgia State University  
PO Box 3992  
Atlanta, GA 30302-3992  
and NBER  
gheutel@gsu.edu

Juan B. Moreno-Cruz  
University of Waterloo  
School of Environment, Enterprise  
and Development  
juan.moreno-cruz@uwaterloo.ca

Soheil Shayegh  
RFF-CMCC European Institute on Economics  
and the Environment  
BASE Milano  
Via Bergognone, 34  
20144 Milano MI  
Italy  
soheilsh@gmail.com

# 1 Introduction

Under current trajectories of greenhouse gas emissions, there exists only about a 5% chance of achieving the Paris Agreement’s goal of limiting the global mean surface temperature increase to “well below” 2°C above pre-industrial levels by 2100 (Raftery et al., 2017). The inertia of the climate system makes achieving this goal through emissions abatement alone a formidable challenge (Fitzpatrick and Kelly, 2017; Brown et al., 2019). Hence solar geoengineering (SGE), which has the potential to slow global warming relatively quickly, has gained popularity among some policy makers and researchers. Some SGE techniques mimic the climate impact of major volcanic eruptions by injecting reflective particles into the upper atmosphere to block and reflect solar radiation back into the space (Ramaswamy et al., 2018). SGE presents a number of difficulties.<sup>1</sup> Nonetheless, SGE is inexpensive and conceptually attractive, and a significant part of the optimal policy in many integrated assessment models.<sup>2</sup>

Here we consider an aspect of SGE not previously studied in integrated assessment modeling: the potential for endogenous learning over uncertainties surrounding SGE and the climate. We focus on two sources of uncertainty. The first is uncertainty about SGE effectiveness, which determines the temperature reduction from a given amount of SGE. The second is uncertainty about climate sensitivity, which is the equilibrium temperature increase resulting from a doubling of atmospheric carbon concentration. Both of these uncertainties are endogenous, so active learning or experimentation is possible. We study optimal experimentation with SGE, both theoretically and computationally with an integrated assessment model.

Intuition suggests that implementing SGE can increase our knowledge about it, since implementation is a type of field experiment. However, given the calibrated current initial conditions, we find a surprising result: implementing SGE actually slows learning about both SGE effectiveness and climate sensitivity, resulting in a less-informed decision. We decompose SGE’s impact on learning into two effects. A *signal strength effect* comes from the effect of SGE on the temperature signal. If the signal strength effect is positive, then SGE makes the temperature change larger in magnitude and thus more visible amidst the noisy weather shocks, speeding learning. However, a

---

<sup>1</sup>For example, SGE performed via injecting sulfur particles causes harmful side effects (Keller et al., 2014; Proctor et al., 2018; Abatayo et al., 2020), does not reduce impacts like ocean acidification that are caused directly by CO<sub>2</sub>, and has a relatively short half life, necessitating frequent injections. See Klepper and Rickels (2014) and Heutel et al. (2016a) for reviews of the economics of solar geoengineering. For a review of the science of SGE, see National Research Council, et. al. (2015). For a broader review of the social science of SGE, see Flegal et al. (2019).

<sup>2</sup>For example, Heutel et al. (2018) shows that optimal SGE policy reduces up to 50% of the radiative forcing (instantaneous warming effect) from CO<sub>2</sub>.

small or medium-scale SGE deployment moves the temperature change closer to zero, and so the signal strength effect is negative, slowing learning about both SGE effectiveness and climate sensitivity. Only an unrealistically large SGE deployment causes a temperature change large enough in absolute value to create a positive signal strength effect which speeds learning. Second, a *noise amplification effect* causes the climate system to be more variable and slows learning about climate sensitivity (though does not affect learning about SGE effectiveness). Because the effectiveness of SGE deployment in reducing the temperature is uncertain, SGE causes the climate system to be more subjectively variable, slowing learning.

We then compute optimal SGE and abatement policies in an integrated assessment model (IAM) with endogenous learning. By “optimal,” we mean the policy path that maximizes the sum of discounted utility, given the costs and benefits of SGE, abatement, and climate change. Our IAM extends the well-known DICE model (Nordhaus, 2016) in several ways. First, in our model SGE is available as an additional policy tool. Second, we model uncertainty over two features of the model: climate sensitivity and SGE effectiveness. We calibrate SGE effectiveness and its uncertainty using volcano eruption data. Third, the planner learns endogenously and updates beliefs over time as a result of SGE deployment and greenhouse gas (GHG) abatement.<sup>3</sup> The computational results show that optimal SGE deployment is never large enough to produce informational gains, and in fact the information loss acts as a disincentive to using SGE. Some SGE is still optimal because of its other benefits. Thus, SGE is used despite of, not because of, its effect on learning. Optimal SGE is highly sensitive to beliefs about climate sensitivity and SGE effectiveness. In the median optimal simulation, SGE usage offsets at most 4% of the radiative forcing from CO<sub>2</sub>. However, when beliefs are that climate change is severe and can be effectively reduced via SGE, deployment increases to 14%. This is consistent with the idea of using SGE as a last resort if climate change becomes severe, although the planner still uses a small amount of SGE even when beliefs are that the climate sensitivity is low.

The type of SGE experiment we consider is a planet-wide implementation. Our results show that a large-scale, planet-wide implementation experiment speeds learning but is not optimal because of the deployment costs and harmful side effects. Our results also show that a small-scale, planet-wide implementation experiment slows learning but is nonetheless optimal. Other types of experiments

---

<sup>3</sup>In the terminology of LaRiviere et al. (2018), we model active adaptive management, since learning is taken into account when making decisions.

are also possible. For example, researchers may glean information from laboratory and/or localized, rather than planet-wide, field experiments of the kind suggested by Keith et al. (2014). Our model does not consider such experiments and thus reaches no conclusions about their optimality or effect on learning.<sup>4</sup>

A large body of literature examines optimal GHG abatement policy when climate processes are uncertain and learning reduces uncertainty over time.<sup>5</sup> Lemoine and Rudik (2017) provide an overview of the literature and methods used in dealing with uncertainty and learning in IAMs. For example, Kelly and Kolstad (1999) model Bayesian learning about climate sensitivity and find that learning takes up to 100 years to become informative. Leach (2007) considers uncertainty over a parameter governing the persistence of temperature, also finding that learning is very slow. Jensen and Traeger (2013) incorporate Bayesian learning in the DICE model, and Lemoine and Traeger (2014) add climate tipping points and allow for learning about the tipping point temperature threshold. Other studies have extended the model to include fat-tailed uncertainty (Kelly and Tan, 2015; Shayegh and Thomas, 2015; Hwang et al., 2017).

In general, the literature finds learning is relatively slow.<sup>6</sup> Therefore, near-term abatement policy with learning is similar to policy without learning. Our paper builds upon this literature by showing that, in an environment with multiple uncertainties, SGE experimentation can actually slow learning by magnifying uncertainty in the climate system. Overall learning about SGE effectiveness is slow, because optimal SGE levels are relatively small.

Several studies introduce SGE into IAMs. Bickel and Lane (2009), Gramstad and Tjøotta (2010), Goes et al. (2011), and Bickel and Agrawal (2013) modify the DICE model to incorporate SGE, but without allowing for epistemic uncertainty. Emmerling and Tavoni (2018) use a different IAM, WITCH, and incorporate SGE, with uncertainty modeled as a binary probability outcome.<sup>7</sup> Heutel et al. (2016b) analyze the use of SGE with a risk of tipping points, and Helwegen et al. (2019) add the possibility of solar radiation management failure in their analysis. Most closely related to this paper, Heutel et al. (2018) modify the DICE model and allow for general forms of epistemic uncertainty. They demonstrate how uncertainty over climate sensitivity and SGE damages affects

---

<sup>4</sup>Both types of learning are necessary. Laboratory experiments generate important predictions, that ultimately must be tested in the uncontrolled, planet-wide environment.

<sup>5</sup>See Pastor et al. (2020); LaRiviere et al. (2018) for literature reviews of uncertainty in climate economic modeling.

<sup>6</sup>Hwang et al. (2019) shows that active learning through knowledge acquisition (e.g. investment in more accurate climatic observations) can reduce uncertainty more rapidly than passive learning.

<sup>7</sup>Other papers study uncertainty over SGE but not in the framework of IAMs. Moreno-Cruz and Keith (2013) model uncertainty with a binary outcome using an analytical model. See Kravitz and MacMartin (2020) for a review of key uncertainties in SGE.

optimal policy. Our paper advances this literature by (1) considering a previously unexplored uncertainty, SGE effectiveness, in addition to climate sensitivity, (2) calibrating SGE effectiveness and uncertainty using volcano data, (3) considering the effect of endogenous learning on SGE policy, and (4) considering SGE when the climate sensitivity is uncertain. Under these extensions, optimal SGE deployment falls considerably relative to the prior literature, from a maximum of about 50% of radiative forcing to a maximum of less than 4%.

## 2 Model

Our IAM is based on the Dynamic Integrated Climate-Economy (DICE) model (Nordhaus, 2016). Heutel et al. (2018) modified DICE to include SGE; here we extend that modification of DICE to also include endogenous learning about climate sensitivity and SGE effectiveness. We adopt the methodology of Traeger (2014), which reduces the dimension of the state space. In particular, we update the parameters given in Traeger (2014) to match the 2016 version of DICE. More details about the original DICE model and its modification to include SGE are included in the above-cited papers. The full model is detailed in Appendix A. In this section we focus on the introduction of endogenous learning to the model.

### 2.1 Overview

DICE is a representative agent model of the global economy and climate. The economic portion of the model is a standard aggregate growth model, with an evolving capital stock, exogenous growth in total factor productivity and in population, and an endogenous choice of the optimal amount of consumption and investment to maximize the net present value of the sum of utility based on per-capita consumption. This economic portion is integrated with a climate model, in which the carbon emissions generated from economic production affect the carbon stock of the atmosphere and oceans, and the atmospheric carbon stock in turn affects average temperatures. Finally, temperature affects the economy through a damage function, in which net output deviates from gross output based on the loss from temperature impacts.

The climate policy choice variable in the original DICE model is abatement  $\alpha$ , which is a number between 0 and 1 representing the fraction of total carbon emissions abated.<sup>8</sup>

---

<sup>8</sup>In DICE,  $\alpha$  may eventually be greater than one, reflecting carbon capture technologies. Here we impose  $\alpha \leq 1$  to

The extension of DICE to allow SGE adds a second policy variable, solar geoengineering  $g$ . This policy variable is normalized so that  $g$  corresponds to the fraction of the radiative forcing  $F$  that is reduced by SGE. Radiative forcing is the difference between the incoming solar heat energy and outgoing energy radiated from Earth. When radiative forcing is positive, the planet will warm because more energy is entering than is leaving. When  $g = 0$ , the radiative forcing is unchanged by SGE. When  $g = 1$ , radiative forcing is reduced by a fraction  $1 - \phi$ , where  $\phi$  measures how effective SGE is at reducing radiative forcing. Unlike the abatement policy variable  $\alpha$  which must be between 0 and 1, SGE  $g$  can take any value greater than 0. If  $g > 1/\phi$ , then SGE more than offsets the warming effect caused by greenhouse gases, and the planet will cool even faster than if GHG concentrations immediately return to pre-industrial levels.

## 2.2 SGE Costs and Damages

Following Heutel et al. (2018), we posit the following model of costs and damages:

$$Y = (1 - \Lambda - D) Q, \quad (1)$$

$$\Lambda = \theta_1(t) \alpha^{\theta_2} + \theta_{GE} g^{\theta_3}, \quad (2)$$

$$D = \pi_T T_{AT}^2 + \pi_m (M - M_{1750})^2 + \pi_g g^2, \quad (3)$$

where  $Q$  is gross world output,  $Y$  is world output net of damages,  $D$ , and spending on emissions abatement and SGE,  $\Lambda$ . The cost function  $\Lambda$  gives the percentage of output spent on emissions abatement and SGE. The cost of a backstop technology which eliminates all carbon emissions,  $\alpha = 1$ , is  $\theta_1(t)$ , which falls exogenously over time. In our notation, functions of time are variables that evolve exogenously over time. We suppress the time dependence of endogenous variables, and use primes to denote next-period values.

Nordhaus (2016) combines damages associated with higher carbon stocks and temperatures into a single function of atmospheric temperature. However, since SGE directly affects temperature while abatement directly affects the carbon stock, we use the damage function (3), which is a function of both the deviation of atmospheric temperature from recent averages,  $T_{AT}$ , and the stock avoid having too many speculative technologies.

of atmospheric carbon  $M$  above preindustrial levels  $M_{1750}$ .<sup>9</sup> Following Heutel et al. (2018), we also include damages caused directly by SGE  $g$  in the damage function (for example, warming of the tropical cold-point tropopause leading to the depletion of the ozone layer Heckendorn et al., 2009).

### 2.3 Carbon Cycle, Radiative Forcing, and Temperature

Following Traeger (2014), the carbon cycle evolves according to:

$$E = \sigma(t)(1 - \alpha)Q + E_{LAND}(t), \quad (4)$$

$$M' = M_{1750} + (1 - \delta_m(t))(M - M_{1750}) + E, \quad (5)$$

Here  $E$  is carbon emissions,  $\sigma(t)$  is the emissions intensity of output, and  $E_{LAND}(t)$  are exogenous emissions from land use changes. In equation (5),  $\delta_m(t)$  is the fraction of atmospheric carbon absorbed by the biosphere and deep ocean. The exogenous absorption rate declines over time as the oceans become more saturated with carbon.

Radiative forcing  $F$  is given by:

$$F' = \left( \eta \log_2 \left[ \frac{M'}{M_{1750}} \right] + F_{EX}(t+1) \right) (1 - \phi g), \quad (6)$$

Here  $\eta$  is the forcing coefficient for carbon and  $F_{EX}(t)$  is exogenous forcing from other greenhouse gasses and aerosols. Let  $\phi \in [0, 1]$  denote the parameter which determines how effective SGE is at reducing radiative forcing.<sup>10</sup>

Atmospheric temperature evolves according to:

$$T'_{AT} = T_{AT} + \xi_1 \left\{ F' - \xi_2 T_{AT} - \xi_3 [T_{AT} - T_{LO}](t) \right\} + \epsilon'. \quad (7)$$

Here  $\xi_1$  governs the speed at which the temperature adjusts to changes in radiative forcing. The temperature differential between the ocean and atmosphere,  $[T_{AT} - T_{LO}](t)$  is exogenous as in Traeger (2014). The parameter  $\xi_2$  measures the magnitude of feedback effects. For example, as the tem-

<sup>9</sup>Traeger (2014) replaces the endogenous stock of carbon in the ocean with an exogenous function that determines carbon absorption by the ocean and biosphere. Hence, we combine the damages from ocean and atmospheric carbon into just a function of atmospheric carbon.

<sup>10</sup>Here SGE affects radiative forcing through a multiplicative effect, as modeled in Heutel et al. (2018). Other papers instead model SGE as affecting radiative forcing through an additive term. Heutel et al. (2018) demonstrate that this modeling choice has little effect on optimal policy outcomes (see their Figure 6 and Appendix Figure A12).



perature rises, ice melts, reducing the albedo effect, causing still higher temperatures (a positive feedback). We thus call  $\xi_2$  the *feedback parameter*. Finally,  $\epsilon$  is a random weather shock.

The *climate sensitivity*  $\Delta T_{2\times}$  is defined as the equilibrium increase in temperature that would arise from a doubling of the pre-industrial carbon stock, without any SGE. Combining equations (6) and (7) at the steady state implies the climate sensitivity is  $\Delta T_{2\times} = \eta/\xi_2$ . As described below, we model uncertainty in the climate sensitivity through uncertainty in the feedback parameter.

The timing is such that both CO<sub>2</sub> and SGE affect radiative forcing in  $t + 1$ , and therefore the temperature in  $t + 1$ .

## 2.4 Uncertainty

We model two sources of uncertainty, one over SGE and one over the climate system. First, we allow the SGE effectiveness parameter,  $\phi$ , to be uncertain. The planner treats  $\phi$  as a random variable  $\tilde{\phi}$ . A given quantity of SGE  $g$  has an uncertain effect on forcing due to uncertainties in how long the sulfur particles will remain in the stratosphere, how well sulfur particles mix across the globe, and effects on cloud formation.<sup>11</sup>

Second, we model uncertainty in the climate sensitivity by allowing the feedback parameter,  $\xi_2$ , to be uncertain. The planner treats  $\xi_2$  as a random variable  $\tilde{\xi}_2$ . Because climate sensitivity  $\Delta T_{2\times}$  is  $\eta/\xi_2$ , which is a function of  $\xi_2$ , treating the feedback parameter  $\xi_2$  as uncertain implies that climate sensitivity  $\Delta T_{2\times}$  is also uncertain.<sup>12</sup>

We assume that radiative forcing net of SGE,  $\frac{F'}{(1-\phi g)}$ , is not observed, which prevents the planner from instantly learning the effectiveness of SGE by inverting the forcing equation (6). Furthermore, the random weather shock prevents the planner from immediately learning the true feedback parameter by inverting the temperature equation (7).

A change of variables simplifies the above equations. Let  $H'$  denote the residual after removing

<sup>11</sup>We do not explicitly model uncertainty in the parameter representing damages from SGE,  $\pi_g$ . This is analogous to the choice of learning over the climate sensitivity rather than over the climate damages. See the 2013 IPCC report for a discussion of the extensive uncertainty with respect to SGE effectiveness. To our knowledge, this paper is the first to analyze uncertainty over SGE effectiveness.

<sup>12</sup>While most of the literature models climate sensitivity uncertainty through uncertain feedbacks (e.g. Roe and Baker, 2007; Kelly and Tan, 2015), this is not the only way to model uncertainty in climate sensitivity. Kelly and Kolstad (1999) and Heutel et al. (2018) model climate sensitivity uncertainty by assuming that the forcing parameter  $\eta$  is uncertain, not the feedback parameter  $\xi_2$ .

the known influences on next-period temperature  $T'_{AT}$ .

$$\begin{aligned} H' &\equiv T'_{AT} - \xi_1 \left( \eta \log_2 \left[ \frac{M'}{M_{1750}} \right] + F_{EX}(t+1) \right) + \xi_1 \xi_3 [T_{AT} - T_{LO}](t) \\ &= -\xi_1 \left( \eta \log_2 \left[ \frac{M'}{M_{1750}} \right] + F_{EX}(t+1) \right) g\tilde{\phi} + (1 - \xi_1 \tilde{\xi}_2) T_{AT} + \epsilon'. \end{aligned} \quad (8)$$

Let  $\hat{F}'$  denote gross forcing before SGE

$$\hat{F}' \equiv \xi_1 \left( \eta \log_2 \left[ \frac{M'}{M_{1750}} \right] + F_{EX}(t+1) \right) \quad (9)$$

and  $\tilde{\beta}$  denote the inertia of the temperature, which we call the *net feedback parameter*:

$$\tilde{\beta} \equiv 1 - \xi_1 \tilde{\xi}_2. \quad (10)$$

Equation (7) then simplifies to:

$$H' = \tilde{\beta} T_{AT} - \tilde{\phi} \hat{F}' g + \epsilon'. \quad (11)$$

This implies that

$$\Delta T_{2\times} = \frac{\eta \xi_1}{1 - \tilde{\beta}}. \quad (12)$$

Equation (11) is a linear regression equation in which the planner tries to determine for example, whether an unusually high temperature (relative to the known underlying carbon forcing and ocean effects) occurs because the feedback effects are stronger than expected, SGE is less effective than expected, or the weather shock was unusually high.

## 2.5 Learning

The weather shock is normally distributed,  $\epsilon' \sim N(0, \rho_\epsilon^{-1})$ , where  $\rho_\epsilon$  is the precision (inverse of the variance). The planner has prior beliefs that the true net feedback parameter is drawn from a normal distribution (Roe and Baker, 2007), and the same for the SGE effectiveness parameter:

$$\begin{bmatrix} \tilde{\beta} \\ \tilde{\phi} \end{bmatrix} \sim N[\mu, P^{-1}], \quad \mu \equiv \begin{bmatrix} \beta \\ \phi \end{bmatrix}, \quad P \equiv \begin{bmatrix} P_1 & P_2 \\ P_2 & P_3 \end{bmatrix}. \quad (13)$$

Here  $\beta$  and  $\phi$  are the means of the prior distributions and  $P$  is the precision of the prior beliefs. We assume  $P$  is positive definite, which is the case if the priors are formed using a variance-covariance matrix.

Bayes' theorem implies that, after observing  $H'$ , the posterior distribution remains bivariate normal, with mean and precision:

$$P' = P + \rho_\epsilon X \cdot X^{tr}, \quad (14)$$

$$\mu' = (P')^{-1} (P\mu + \rho_\epsilon XH') \quad (15)$$

$$X \equiv \begin{bmatrix} T_{AT} \\ -\hat{F}'g \end{bmatrix} \quad (16)$$

Here  $tr$  denotes the transpose operator. The planner can manipulate the second element of  $X$  directly through the SGE policy choice,  $g$  and indirectly through the abatement policy choice,  $\alpha$ .<sup>13</sup> Thus, learning is endogenous. However, the first element of  $X$ ,  $T_{AT}$ , is already determined at the start of period  $t$  and thus unaffected by the choice of SGE and abatement in period  $t$ . It is natural to assume  $P_1 > 0$ ,  $P_3 > 0$ , and  $P_2 \leq 0$  given that  $P_2$  evolves over time as the sum of observations on  $-T_{AT}\hat{F}g$ , which is negative.

Finally, a critical feature of the model is that  $T'_{AT}$  and  $H'$  are sums of normal random variables and are therefore also normally distributed.

$$H' \sim N [\mu_H, P_H^{-1}] \quad (17)$$

$$\mu_H = X^{tr} \cdot \mu \quad (18)$$

$$P_H^{-1} = X^{tr} \cdot P^{-1} \cdot X + \rho_\epsilon^{-1} \quad (19)$$

Therefore, a single numerical integration with respect to the normal random variable  $H$  is sufficient for computing the expectation of the value function. More importantly, the variability of the climate as perceived by the planner (i.e. considering both stochasticity and uncertainty) is a function of SGE deployment. We will show that this magnification of variability caused by SGE can slow learning.

<sup>13</sup> $\hat{F}'$  is a function of  $M'$  via equation (6) which is a function of emissions  $E$  via equation (5) and abatement  $\alpha$  via equation (4).

### 3 Theoretical Predictions

Before presenting the numerical simulation results, we present some theoretical propositions about learning that illuminate the model's predictions. Proofs of all propositions are in Appendix B.

It will sometimes be more convenient to work with the prior variance-covariance  $W$  rather than the precision  $P$ . Let:

$$W = P^{-1} \equiv \begin{bmatrix} W_1 & W_2 \\ W_2 & W_3 \end{bmatrix}. \quad (20)$$

Evaluating the posterior variance-covariance,  $W'$ , of the belief distribution over the uncertain variables  $\tilde{\beta}$  and  $\tilde{\phi}$  after observing  $H'$  reveals that:<sup>14</sup>

$$W' = \frac{1}{1 + \rho_\epsilon X^{tr} W X} \begin{bmatrix} W_1 + \rho_\epsilon |W| X_2^2 & W_2 - \rho_\epsilon |W| X_1 X_2 \\ W_2 - \rho_\epsilon |W| X_1 X_2 & W_3 + \rho_\epsilon |W| X_1^2 \end{bmatrix}. \quad (21)$$

SGE,  $g$ , directly affects  $X_2 = -\hat{F}'g$ , and abatement,  $\alpha$ , indirectly affects  $X_2$ . Therefore equation (21) shows both current-period policy variables affect the posterior variance of the estimates for both  $\tilde{\beta}$  and  $\tilde{\phi}$  through their effect on  $X_2$ . By contrast, the policy choices  $g$  and  $\alpha$  do not affect  $X_1 = T_{AT}$ , which is already determined at the start of the period.

We want to identify conditions under which SGE use unambiguously increases information, and likewise for the use of abatement. To do so, we first establish conditions under which the terms in the variance-covariance matrix (21) are decreasing over time. This result also creates natural bounds for the variance states in the computational algorithm and signs the elements of  $P$  and  $W$  for the later propositions. Replace the prime notation with  $t$  subscripts, where  $W_t$  represents the variance-covariance matrix of beliefs at time  $t$ , and  $W_0$  represents it at the initial period. Let  $W_{i,t}$  represent the value of the  $i$ th element of  $W_t$ . We restrict the prior variance-covariance matrix  $W_0$  to be positive-definite. Starting from a diffuse prior,  $P_0 = 0$ , (as would be the case in an OLS regression), equation (14) implies that  $P_t$  and therefore  $W_t$  are positive-definite for all  $t$ . Without this restriction, it is possible to construct examples where the variances can become negative or unbounded. With this assumption, we can show:

**PROPOSITION 1** *Let  $W_{1,0} > 0$ ,  $W_{2,0} > 0$ ,  $W_{3,0} > 0$ , and  $|W_0| > 0$ . Then:  $0 \leq W_{1,t} \leq W_{1,0}$ ,  $0 \leq W_{3,t} \leq W_{3,0}$ ,  $0 \leq W_{2,t} \leq (W_{1,0}W_{3,0})^{\frac{1}{2}}$  and  $|W_t| > 0$  for all finite  $t$ . Further,  $W_{i,t+1} \leq W_{i,t}$  for*

<sup>14</sup>See equation (A.49) in the appendix.

$i = 1, 3$ . That is, the planner gains information after each observation.

Proposition 1 shows the variance-covariance matrix terms remain on finite intervals, which is necessary for convergence of the computational algorithm. More importantly, Proposition 1 shows that, regardless of the decisions, the planner gains information each period ( $W_{1,t+1} < W_{1,t}$  and  $W_{3,t+1} < W_{3,t}$ ).

### 3.1 Learning from SGE

Although the planner gains information with each observation over time, the policy decisions affect the amount of information gained. In fact, whether an increase in SGE speeds or slows learning about either of the two unknown variables  $\tilde{\beta}$  and  $\tilde{\phi}$  depends on the level of SGE relative to the current information state. We will show below that there are two threshold values of SGE, defined as  $I_1$  and  $I_2$ , that determine the direction of the effect on SGE on learning.

First, consider the effect of SGE on the posterior variance of belief over the SGE effectiveness parameter  $\phi$ . This variance in period  $t + 1$  is  $W_{3,t+1}$ , which we will now denote as  $W'_3$ . An increase in SGE speeds learning about SGE effectiveness if the partial derivative of  $W'_3$  with respect to  $g$  is negative. We show in Appendix B.2 that:

$$\frac{\partial W'_3}{\partial g} = \frac{\hat{F}\rho_\epsilon 2W'_3}{1 + \rho_\epsilon X^{tr}WX} (W_2 T_{AT} - W_3 \hat{F}'g) \quad (22)$$

$$\frac{\partial W'_3}{\partial g} < 0, \Leftrightarrow g > I_1 \equiv \frac{W_2}{W_3} \cdot \frac{T_{AT}}{\hat{F}'}. \quad (23)$$

SGE  $g$  increases learning about SGE effectiveness if and only if the level of SGE exceeds the threshold value  $I_1$ . To understand the intuition, it is helpful to view (11) as an OLS regression equation.<sup>15</sup> Suppose a given set of past decisions results in a data set which is used to estimate  $\beta$  and  $\phi$  using (11), with associated variance-covariance matrix (20). Now the planner has the opportunity to alter the current SGE and thus the current  $X_2$ , and then re-run the regression with the past and current data. How does changing  $g$  affect the variance of the parameter estimates?

Suppose SGE is increased from a low baseline close to zero. The increase in SGE has a negative effect on temperature which cancels with the positive feedback effect ( $\beta X_1$ ). The resulting signal  $H'$  is smaller relative to the noisy weather shock. The planner has low confidence that the temperature

<sup>15</sup>In fact, it is straightforward to show that (21) is identical to the variance-covariance matrix of the OLS parameter estimates with known  $\sigma_\epsilon^2$ , for appropriately chosen priors  $P_1 = \sigma_\epsilon^2 \sum_{i=0}^{t-1} X_{1,i}$  and analogously for  $P_2$  and  $P_3$ .

change resulted from SGE. Hence, as SGE increases, the signal becomes smaller, the new information is less informative, and  $W'_3$  changes less.

Suppose instead that SGE is increased from a high baseline. In this case, the planner expects a large temperature reduction due to SGE, and further increases in SGE start to make the temperature signal  $H'$  larger in magnitude (more negative). It is then increasingly unlikely that the temperature change is the result of a large negative weather shock. The planner attributes the change in temperature to SGE with high confidence, and thus the data point is highly informative, and the variance falls as SGE rises.

We denote the nonlinear effect of SGE on  $H'$  as the *signal strength effect*. The signal strength effect is quadratic in  $g$ : an increase in  $g$  from a small baseline cancels with the feedback effects weakening the signal. Increasing  $g$  from a large baseline more than the threshold  $I_1$  swamps the feedback effect, strengthening the signal.<sup>16</sup> Equation (22) shows that increasing SGE strengthens the signal for a baseline  $g > I_1$ . The cutoff  $I_1$  depends on temperature since if the temperature is larger, so is the feedback effect which must be overcome. Conversely, if forcing is large, then SGE has a large effect on temperature which more easily swamps the feedback effect. The cutoff  $I_1$  also depends on the pre-existing uncertainty, for example, if  $W_2$  is small it is easier to separate the feedback and SGE effects, and so a smaller temperature change is more easily attributed to the change in SGE.

Next, consider the effect of SGE on the posterior variance  $W'_1$ , which is the variance of beliefs about the net feedback parameter  $\beta$ . We show in Appendix B.2 that:

$$\frac{\partial W'_1}{\partial g} = \frac{\hat{F}\rho_\epsilon 2W'_2}{1 + \rho_\epsilon X^{tr}WX} (W_1 T_{AT} - W_2 \hat{F}'g), \quad (24)$$

$$\frac{\partial W'_1}{\partial g} < 0, \Leftrightarrow g > I_2 \equiv \frac{W_1}{W_2} \cdot \frac{T_{AT}}{\hat{F}'}. \quad (25)$$

SGE  $g$  increases learning about the net feedback parameter if and only if the level of SGE exceeds the threshold value  $I_2$ . SGE affects the signal strength  $H'$  in an identical, quadratic way. The signal strength effect on learning about feedbacks is proportional to the signal strength effect on learning about SGE effectiveness. However, SGE has an additional effect on learning about feedbacks, which we call the *noise amplification effect*. Increasing SGE from any baseline increases the subjective noise in the climate system when trying to estimate the feedback effect. In particular, the effect

<sup>16</sup>Mathematically, in (21),  $1 + \rho_\epsilon X^{tr}WX$  is quadratic in  $g$ , and so  $g$  has a quadratic effect on  $W'$ .

of feedbacks on temperature is now obscured not only by the noisy weather shock, but also by an uncertain SGE effect. The planner is now uncertain if (say) a warm year was caused by stronger than expected feedbacks, weather noise, or SGE being less effective than expected. This noise amplification effect slows learning about feedback effects, all other things equal.<sup>17</sup>

Appendix B.2 shows  $I_2 > I_1$ . That is, the noise amplification effect implies the baseline  $g$  must be larger for SGE to speed learning about feedbacks relative to SGE effectiveness, as the signal strength effect must not only be positive, but also overcome the noise amplification effect.

The following proposition summarizes the above discussion on the role of SGE on learning:

**PROPOSITION 2** *Let  $W_{1,0} > 0$ ,  $W_{2,0} > 0$ ,  $W_{3,0} > 0$ , and  $|W_0| > 0$ . Then  $I_1 \leq I_2$  for all finite  $t \geq 0$  and up to three regions exist:*

- *Region 1:  $g < I_1$ . In this region an increase in SGE increases posterior uncertainty for both  $\tilde{\beta}$  and  $\tilde{\phi}$ .*
- *Region 2:  $I_1 \leq g < I_2$ . In this region an increase in SGE decreases uncertainty over  $\tilde{\phi}$  but increases uncertainty over  $\tilde{\beta}$ .<sup>18</sup>*
- *Region 3:  $g \geq I_2$ . In this region an increase in SGE decreases uncertainty for both  $\tilde{\beta}$  and  $\tilde{\phi}$ .*

Proposition 2 shows that sufficiently small SGE experiments slow learning, whereas sufficiently large SGE experiments speed learning. To understand the magnitude of the SGE experiment required to speed learning, we can use the calibrated initial values to recover the current period  $I_1$  and  $I_2$ . Details on the calibration of the initial conditions of the model are presented in Appendix D. Given those calibrated parameters, we calculate the initial values of the variables defining the cutoff regions:  $I_1 = 7.34$ , and  $I_2 = 114.1$ .<sup>19</sup> Hence only for  $g > I_1 = 7.34$  will experimentation with SGE speed learning about the net feedback parameter. Since  $g$  is normalized so that  $g = 1$  corresponds to about 5MT of sulfur, to speed learning would require a massive experiment of about 36.7MT of sulfur.<sup>20</sup> Thus, for any reasonably-sized implementation of SGE experiment, on the scale of what is being proposed by policy makers and IAMs, SGE will slow learning about both the net

<sup>17</sup>Mathematically, the noise amplification effect is the second term in the numerator of  $W'_1$  given in equation (22).

<sup>18</sup>Region 2 can be further decomposed into two subregions where SGE has differential effects on the covariance  $W'_2$ . See Appendix B.2.

<sup>19</sup>This comes from the fact that  $\frac{T}{F'} = \frac{0.85}{0.54} = 1.57$ , and  $W_1 = 0.13^2$ ,  $W_2 = 0.0153^2$ , and  $W_3 = 0.007^2$ . Thus  $\frac{W_2}{W_3} = 4.67$  and  $\frac{W_1}{W_2} = 72.6$ .

<sup>20</sup>For reference, the Mount Pinatubo eruption in 1982 injected an estimated 20MT of sulfur and significantly cooled global temperatures.

feedback parameter,  $\tilde{\beta}$ , and the effectiveness of SGE,  $\phi$ . There is no justification for small-scale, planet-wide SGE experimentation based on reducing uncertainties, at least at the current calibrated conditions. Later, in the numerical simulation results, we explore whether this result holds over time as conditions change.

### 3.2 Learning from Abatement

Consider now the effect of abatement on learning. The next proposition shows that abatement policy,  $\alpha$  and SGE policy,  $g$  have opposite effects on information gain – whenever more SGE decreases posterior uncertainty over an unknown variable, more abatement increases uncertainty over that variable. That is, whenever  $\frac{\partial W'_i}{\partial g} < 0$ , we will have  $\frac{\partial W'_i}{\partial \alpha} > 0$ .

**PROPOSITION 3** *Let  $W_{1,0} > 0$ ,  $W_{2,0} > 0$ ,  $W_{3,0} > 0$ , and  $|W_0| > 0$ . Then*

- *Region 1:  $g < I_1$ . In this region an increase in abatement decreases uncertainty for both  $\tilde{\beta}$  and  $\tilde{\phi}$ .*
- *Region 2:  $I_1 \leq g < I_2$ . In this region an increase in abatement decreases uncertainty over  $\tilde{\beta}$  but increases uncertainty over  $\tilde{\phi}$ .*
- *Region 3:  $g \geq I_2$ . In this region an increase in abatement increases uncertainty for both  $\tilde{\beta}$  and  $\tilde{\phi}$ .*

Increasing SGE decreases  $X_2$  (makes it more negative), while increasing abatement increases  $X_2$  (brings it closer to zero).

Increasing abatement reduces the amount of forcing available for a given level of SGE to act on. SGE becomes less efficient in this sense. Therefore, if SGE is in a region where SGE speeds learning ( $g > I_1$ ), then abatement weakens the positive signal strength effect of SGE, slowing learning. Conversely, if SGE is in a region where SGE slows learning ( $g < I_1$ ), the abatement weakens the negative signal strength effect of SGE, speeding learning.<sup>21</sup>

<sup>21</sup>It is useful to contrast Proposition 3 with the results of Kelly and Kolstad (1999). That paper had only one uncertainty, the forcing parameter,  $\xi_1 \eta$ . From equations (9), (11), and (16), uncertainty about the forcing parameter and uncertainty about SGE effectiveness are both equivalent to uncertainty about the net forcing  $X_2$ . (More gross forcing is equivalent to more net forcing after SGE.) In Kelly and Kolstad (1999), abatement always slowed learning. Here, we have uncertainty about the net feedback parameter in addition to uncertainty about forcing through SGE. Suppose  $W_1 = W_2 = 0$ , so that only net forcing is uncertain. Then it is straightforward to show that  $W'_1 = W'_2 = 0$ . Since the feedback effect is certain, no further learning takes place about it regardless of abatement. Further,  $I_1 = 0$ , so region 2 holds for all  $g$ . In this region, an increase in abatement  $\alpha$  slows learning about SGE effectiveness or equivalently net forcing. Thus, the result of Kelly and Kolstad (1999) emerges as a special case when the prior uncertainty over the net feedback parameter is sufficiently small. When the net feedback parameter uncertainty is large, abatement may speed learning.



Quantitatively, experimentation with abatement is less fruitful than experimentation with SGE. Changes in abatement have only small effects on the current stock of CO<sub>2</sub>, which has built up over centuries. Therefore, changes in abatement have little effect on  $X_2$ . Consider again the calibrated initial condition described in the previous section. If  $\alpha = 0$ , then, from equation (9),  $\hat{F}' = 0.5466$ , and if  $\alpha = 1$ ,  $\hat{F}' = 0.5302$ . Thus,  $I_1$  varies between 7.26 and 7.48, so the planner does not create additional regions by changing  $\alpha$ . Consider the effect of increasing abatement  $\alpha$  from 0 to 1 for a given value of  $g$ . For example, when  $g = 0.1$ :

$$\frac{W'(g = 0.1, \alpha = 1) - W'(g = 0.1, \alpha = 0)}{W'(g = 0.1, \alpha = 0)} = \begin{bmatrix} -0.006\% & -0.08\% \\ -0.08\% & -0.005\% \end{bmatrix}, \quad (26)$$

With  $g$  in region 1, moving from  $\alpha = 0$  to  $\alpha = 1$  speeds learning as indicated by Proposition 3, but the effect is small: the variance terms decrease by less than one hundredth of one percent despite the large increase in abatement.

Thus, the justification for experimentation with abatement to reduce uncertainties is quantitatively small, though of course abatement yields other benefits. The numerical simulations below determine optimal abatement and SGE including all costs and benefits, informational and otherwise.

### 3.3 Trade-off Between Information Gains and Losses

In region 2, SGE increases information over SGE effectiveness  $\tilde{\phi}$  but decreases information over the net feedback parameter  $\tilde{\beta}$ . Ignore for the moment all of the other costs and benefits associated with an SGE experiment, and consider only the effect on uncertainty. Is the information gain worth the information loss? That is, does SGE experimentation result in more accurate decision making and higher utility?

The concept of Blackwell informativeness answers this question. If an SGE experiment results in an uncertainty distribution such that temperature can be predicted more accurately than without such an experiment, then the more accurate prediction leads to higher utility. In this case, the SGE experiment is said to be more Blackwell informative.

The next proposition demonstrates that for  $g > I_1$ , the information gain about SGE effectiveness is worth the information loss about the net feedback parameter, or that Blackwell informativeness is increasing in  $g$ .

**PROPOSITION 4** *Let  $W_{1,0} > 0$ ,  $W_{2,0} > 0$ ,  $W_{3,0} > 0$ , and  $|W_0| > 0$ .*

1. *Consider two posterior distributions  $\Phi_1 = N[\mu'(g_1), W'(g_1)]$  and  $\Phi_2 = N[\mu'(g_2), W'(g_2)]$ , produced from experiments  $g_1$  and  $g_2$ , with  $g_2 > g_1$ . Then experiment 2 is more Blackwell informative than experiment 1 for a given  $X$  if:*

$$\frac{\left(\mu'(g_2)^{tr} X\right)^2}{X^{tr} W'(g_2) X + \rho_\epsilon^{-1}} > \frac{\left(\mu'(g_1)^{tr} X\right)^2}{X^{tr} W'(g_1) X + \rho_\epsilon^{-1}}. \quad (27)$$

2. *Consider two posterior distributions  $\Phi_1 = N[\mu', W'(g)]$  and  $\Phi_2 = N[\mu', W'(g + \Delta g)]$ , where  $\Delta g > 0$ . Then for  $\Delta g$  sufficiently small, experiment 2 is more Blackwell informative than experiment 1 for a given  $X$  if  $g > I_1$ .*

Consider an experiment of increasing SGE policy,  $g$ . Given the normally-distributed prior uncertainty and weather shocks, the problem can be condensed into a single random variable ( $H'$  or  $T'_{AT}$ ).<sup>22</sup> Thus, the posterior distribution is more Blackwell informative if it produces a more accurate prediction of  $T''$  in the next period. Further, a more accurate prediction necessarily results in a more informed decision and therefore higher utility. An increase in SGE makes  $X_2$  more negative, which affects  $W'$  through equation (21). Considering this effect only, the second part of Proposition 4 shows that the information gain regarding  $\tilde{\phi}$  is more valuable than the information loss regarding  $\tilde{\beta}$  in region 2. Therefore, in regions 2 and 3, SGE experimentation on net produces valuable information that leads to more informed decisions.<sup>23</sup>

A change in SGE also affects the mean of the posterior distribution.<sup>24</sup> The first part of Proposition 4 shows that the overall effect on information depends on how SGE affects both the mean and variance of the prior. We can rewrite equation (27) as:<sup>25</sup>

$$\frac{\mu_H(g_2)^2}{\text{var}_H(g_2)} > \frac{\mu_H(g_1)^2}{\text{var}_H(g_1)}. \quad (28)$$

Hence, increasing SGE is more Blackwell informative if doing so increases the signal-to-noise ratio.

SGE experimentation can produce a stronger or a weaker signal. Indeed, since  $\mu'$  depends on the

<sup>22</sup>See equation (17).

<sup>23</sup>The information value of SGE experimentation must be weighed against the cost and damage of implementing SGE, and the benefit in terms of less forcing. This is addressed in the next section.

<sup>24</sup>See equation (15)

<sup>25</sup>From equations (A.48) and (A.55), the signal for  $T'$  is  $E[T'] = \hat{F}' - \xi_1 \xi_3 (T_{AT} - T_{LO})(t) + \mu^{tr} X$ , of which only the last term matters since only the last term depends on  $g$ . Further, equation (A.56) indicates the noise with respect to  $T'$  is  $\text{var}_H$ .

random variable  $\epsilon'$ , the effect of experimentation on the signal varies across periods. Nonetheless, from Bayes' theorem,  $E[\mu'] = \mu$  regardless of  $X$ , so in expectation experimentation has no effect on the signal. Thus, the effect of experimentation on the noise shown in part 2 of Proposition 4 is likely to be quantitatively more important. Finally, the value of  $X$  matters and the informativeness of experimentation varies over time.

## 4 Simulation Results

Propositions 2 and 3 in Section 3 give conditions under which deployment of either SGE or abatement increases the speed of learning over climate sensitivity and/or SGE effectiveness. Given initial conditions, we can say whether there is information value in experimentation with either policy instrument. The theoretical results, however, do not give the optimal paths for both policies, taking into account their informational values as well as all other costs and benefits. To answer that question, we turn to a numerical simulation.

We describe the details of our computational solution method in Appendix C and our calibration in Appendix D. Notably, we use a novel strategy to calibrate SGE effectiveness and uncertainty using data from historical volcanic eruptions. We then run 10,000 simulations of the solved model, each simulation lasting 185 years. We choose 185 years since by the end of that period (the year 2200), all policy values have roughly leveled off for all simulations. All of the certain parameter values are of course identical across each of the 10,000 simulations, and each simulation has the same prior distribution of beliefs about the two uncertain parameters in the initial year. For each simulation, we draw a new true value of  $\tilde{\beta}$  and a new true value of  $\tilde{\phi}$  from that prior distribution. These true values are unknown to the planner, though the planner learns endogenously over time. We also draw a new weather shock  $\epsilon_{it}$  for each simulation  $i$  in each year  $t$ . We report the median value of the policy variables across the 10,000 simulations. These results are the medians conditional on the identical initial (period zero) prior across simulations. These median values will differ from assuming  $\tilde{\beta} = \beta_0$  and  $\tilde{\phi} = \phi_0$ , which would give only the values conditional on the unlikely event that the initial mean belief was exactly correct.

## 4.1 Optimal Policy

Figure 1 plots the median optimal SGE for each period over the 10,000 simulations (red plus symbol). We also plot the median SGE across just the simulations where the planner's current beliefs about the values of the uncertain parameters  $\beta_{it}$  and  $\phi_{it}$  are in the top ten percentiles of the belief distribution (green circles), and the median SGE across just the simulations where the planner's current beliefs  $\beta_{it}$  and  $\phi_{it}$  are in the bottom ten percentiles (blue squares).<sup>26</sup> The green curve thus represents optimal SGE policy conditional on the planner believing that SGE is very effective and climate sensitivity is very high, while the blue curve represents optimal SGE policy conditional on the planner believing that SGE is very ineffective and climate sensitivity is very low.

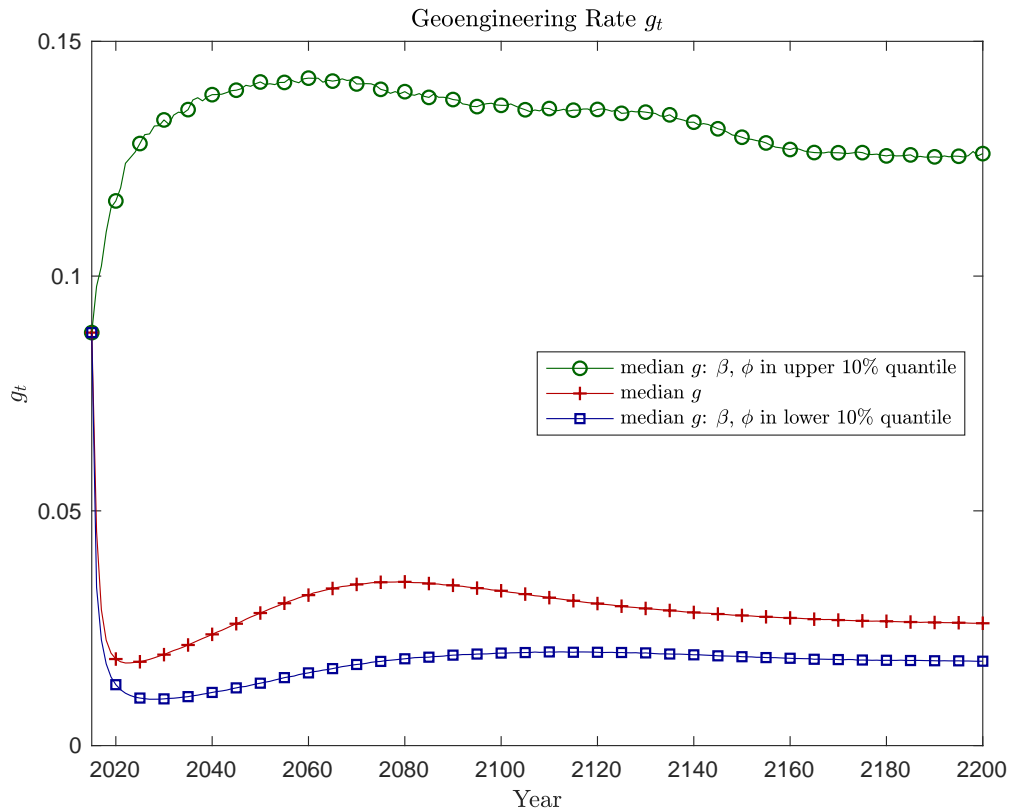


Figure 1: SGE policy,  $g_t$ , 10,000 simulations. Markers are every 5 years for clarity, but the data are annual in all figures.

For the overall median, in 2015 the geoengineering rate  $g$  is 0.088 (offsetting 8.8% of radiative

<sup>26</sup>We require that both  $\beta_{it}$  and  $\phi_{it}$  are in the top ten percentiles of their respective distributions. By definition, 1,000 of the 10,000 simulations have  $\beta_{it}$  in its top ten percentile, and likewise for  $\phi_{it}$ . But only about 300 simulations have both  $\beta_{it}$  and  $\phi_{it}$  in their top ten percentiles. Similarly for the simulations of the bottom ten percentiles.

forcing) and then falls over the next nine years. We will show that initially the planner is concerned about the possibility that the climate sensitivity might be much higher than the initial prior. In most simulations, the planner is able to rule out these worst-case scenarios relatively quickly, and so SGE declines. Hence, initially, a moderate amount of SGE is optimal for precautionary reasons.

The upper and lower quantiles also begin in 2015 at  $g = 0.088$ , since all simulations start with the same initial beliefs and thus the same SGE policy. However, when beliefs are that climate sensitivity and SGE effectiveness are high, optimal SGE rises, peaking at  $g = 0.14$  (offsetting 14% of radiative forcing). Conversely, when beliefs indicate SGE effectiveness and the climate sensitivity are likely to be low, the optimal SGE plummets to 0.01. Optimal SGE is thus highly sensitive to beliefs about the SGE effectiveness and climate sensitivity. SGE is largely a policy used quite sparingly, and only under extraordinary beliefs is SGE deployed at anything more than about  $g = 0.03$ . However, for most beliefs in the first few years there is some SGE for precautionary purposes.

Eventually, the median SGE begins to increase as rising carbon concentrations and wealth makes SGE more attractive, rising to about 0.035, before falling as the substitute policy of abatement becomes increasingly attractive due to its exogenously declining cost. The median optimal SGE is closer to the 10% quantile than the 90% quantile. The climate sensitivity distribution is bounded below by zero but is unbounded above, and the prior distribution is asymmetric and fat-tailed (Kelly and Tan, 2015).

We next compare our results on optimal SGE policy with those of Heutel et al. (2018) (see their Figure 4f). In our model, the initial beliefs (prior mean) of the net feedback parameter and SGE effectiveness are  $\beta_0 = 0.65$  and  $\phi_0 = 0.092$ , respectively. In their model, the mean value of the net feedback parameter is  $\beta_0 = 0.87$  and SGE effectiveness is fixed at  $\phi_0 = 0.5$ . As a result, although in their model optimal geoengineering has the same shape as in our model, SGE rises to about  $g = 0.32$  before declining. In our model in contrast, SGE rises to only  $g = 0.035$ . SGE is used less here relative to the prior literature for three reasons. First, our calibration has an initial belief that effectiveness is only 0.092. Our calibration is very conservative in that we assume SGE effectiveness in reducing temperatures is similar to volcanic eruptions. However, some research indicates careful choice of the location and timing of deployment can increase SGE effectiveness tenfold (e.g. Kravitz et al., 2019). Second, SGE effectiveness is uncertain in our model. Third, SGE at these levels slows learning, leading to less informed decision-making. Even if we solve our model assuming the mean of the prior beliefs of SGE effectiveness is 0.5, SGE peaks at  $g = 0.188$ .

Therefore, uncertain effectiveness and slower learning are quantitatively significant deterrents for SGE deployment, reducing the optimal SGE by about 41% relative to Heutel et al. (2018).

Figure 2 plots the median optimal abatement policy  $\alpha$ , as well as the median abatement policy when beliefs about the net feedback parameter and SGE effectiveness are in the 10th and 90th quantiles.

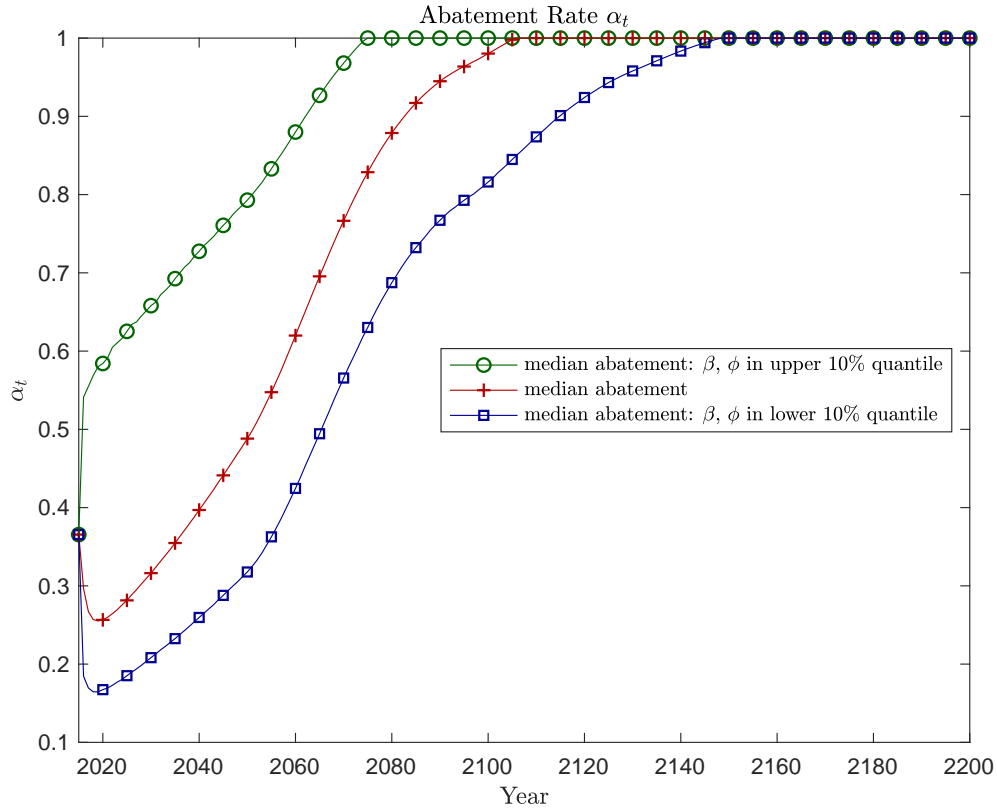


Figure 2: Abatement policy  $\alpha_t$ , 10,000 simulations.

The initial abatement rate is about 37% in 2015. Median optimal abatement subsequently falls to about 26% as learning rules out some of the worst climate sensitivity cases. Then abatement begins to rise again, as the cost of abatement falls to near zero and growth in capital, population, and productivity quickly raise emissions gross of abatement. Eventually abatement is so inexpensive that 100% abatement becomes optimal. This result is consistent with the prior DICE literature.<sup>27</sup>

When beliefs about the climate sensitivity and SGE effectiveness are in the 90th percentile,

<sup>27</sup>Nordhaus (2016) constrains abatement to be less than or equal to 120%, to accommodate modeling carbon dioxide removal (negative emissions), whereas we do not allow for that policy and so set the maximum abatement at 100%.

abatement rises more quickly. Because beliefs are that the climate is very sensitive to carbon, emissions cause higher temperatures and more damage, so higher abatement is optimal. Thus, when beliefs about the climate sensitivity rise, the planner uses more of both SGE and abatement. Because costs are convex, it is less expensive to use some of each rather than one or the other exclusively. Nonetheless, the optimal decision favors abatement, in the sense that the planner is at the margin spending more on abatement for the same temperature reduction as SGE. This is because SGE does not directly reduce damages from CO<sub>2</sub>, creates damages itself, and slows learning. Thus, SGE does not eliminate the need for abatement, a concern expressed in some of the prior literature.

In Appendix E, we show how the forecast errors over the uncertain variables evolve, which illuminates how the speed of learning differs across the variables.

## 4.2 Effect of Learning on Optimal Policy

We explore how uncertainty and learning affect policy by comparing three sets of simulations. First, in the *learning* case, we present the optimal policy simulations under our full model where there is both uncertainty and endogenous learning over two parameters (these are the results presented earlier in Figures 1 and 2). Second, in the *certainty* case, we present analogous optimal policy simulations without uncertainty. That is, we again simulate optimal policy for 10,000 simulations, each of which lasting 185 years, where at the start of each simulation we draw a true value of each uncertain parameter  $\beta$  and  $\phi$  from the prior distribution. But, the prior mean belief is set equal to this true value and the variance of the prior is set equal to zero, so that there is certainty over these values at the start and thus no learning.<sup>28</sup> Third, in the *no-learning* case, we present analogous optimal policy simulations under uncertainty but without learning. To do this, we solve the model such that the planner knows no learning will take place in the future ( $W$  is no longer a state, and beliefs over  $\beta$  and  $\phi$  are fixed at the prior distribution). We again simulate the optimal policy for 10,000 simulations, where at the start of each simulation we draw a true value for  $\beta$  and  $\phi$ , unobserved by the planner. We average 10,000 such paths without learning, to get the expected path conditional on the prior information and no learning.

Figures 3 and 4 present the simulation results for optimal SGE policy. Figure 3 contrasts the certainty and learning simulations, and Figure 4 contrasts the learning and no-learning simulations.

<sup>28</sup>However, a random weather shock is drawn in each period of each simulation, so that even in the certainty case future weather shocks are unknown.

In each figure, we present the median optimal policy, and the median optimal policy when the feedback and SGE effectiveness beliefs are in the 10th and 90th percentile, both for the simulations with learning (circle markers, replicating Figure 1) and for the simulations under either certainty or no-learning (plus markers).

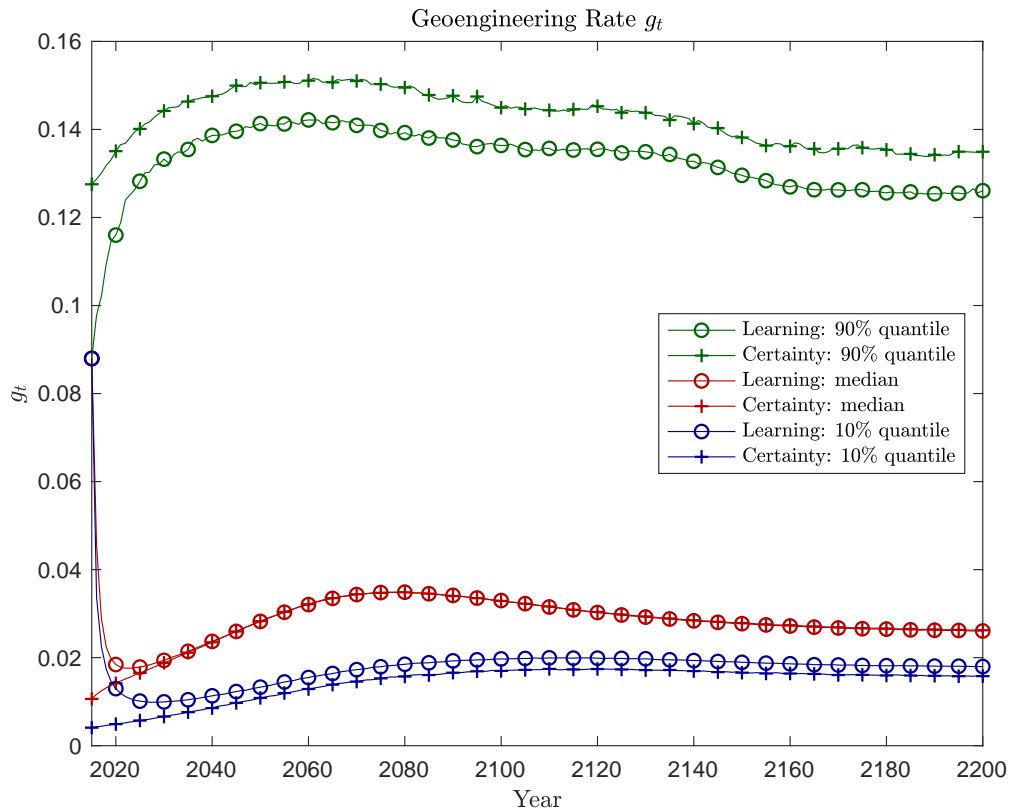


Figure 3: SGE policy,  $g_t$ , 10,000 simulations, learning and certainty cases.

Figure 3 shows that uncertainty matters initially. In 2015 the median SGE policy is  $g = 0.088$ , yet if the planner knew the climate sensitivity and SGE effectiveness were in the 90% quantile, mean SGE policy would be  $g = 0.128$  and if the planner knew the climate sensitivity and SGE effectiveness were in the 10% quantile, median optimal SGE would be near zero ( $g = 0.004$ ). Although the learning policies generally approach the certainty policies as learning resolves, some differences persist since uncertainty regarding SGE effectiveness is slow to resolve. In particular, when SGE is very effective, beliefs are slow to increase, resulting in the learning policy using less SGE than is optimal given certainty, as the planner believes SGE is not as effective as it actually is. Conversely, when SGE is



not very effective, beliefs are slow to decline, and the learning policy uses more SGE than is optimal under certainty as the planner believes SGE is more effective than it actually is.

Figure 3 also shows that the median SGE policy under learning is initially much greater than the certainty policy, as SGE is used initially as a precaution against the possibility that the climate sensitivity is very high. Since learning quickly rules out this case in most simulations, SGE policy becomes similar under the two simulations.<sup>29</sup>

Figure 4 contrasts optimal SGE policy under learning with optimal policy under uncertainty but no learning.

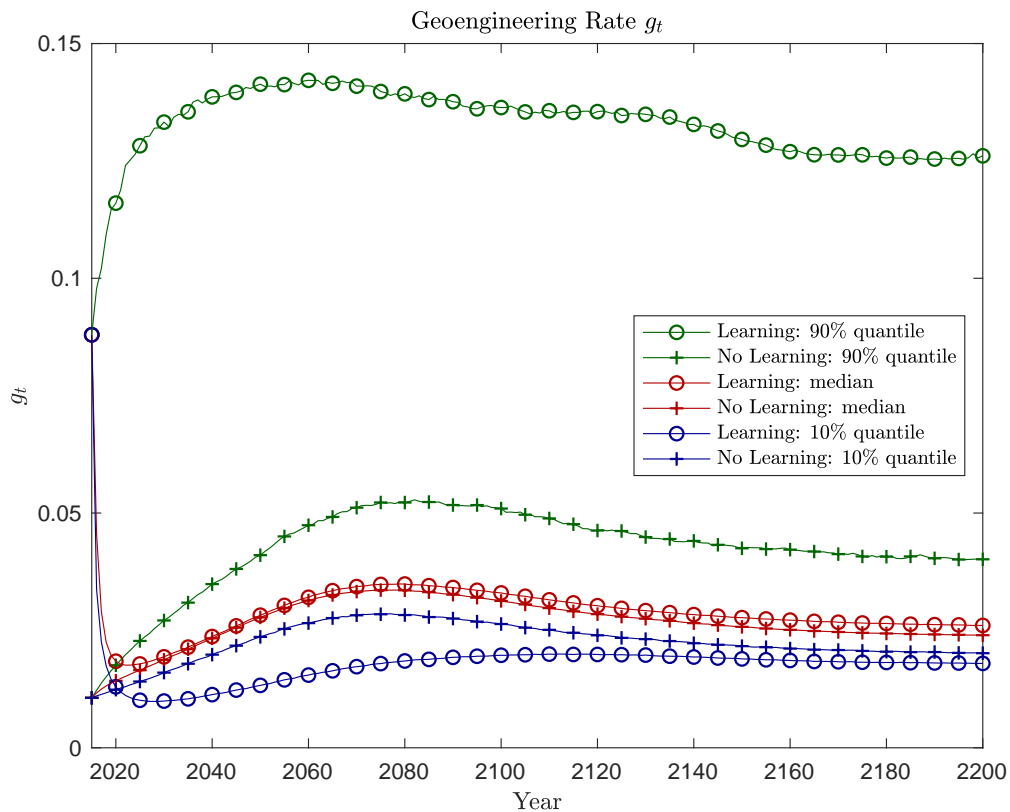


Figure 4: SGE policy,  $g_t$ , 10,000 simulations, learning and no learning.

Because the planner knows that no learning will take place, the initial-period policies differ even though initial beliefs are identical. Initial use of SGE is lower without learning.

As the simulations progress, learning allows the planner to tailor SGE policy, substantially in-

<sup>29</sup>These results are consistent with Kelly and Tan (2015), who also find that mean certainty and uncertainty policies are similar after the first decade.

---

creasing SGE when beliefs indicate climate change is severe and SGE is effective. Even without learning, there is some difference across the three median policies despite no difference in beliefs. This is because temperature differs across the simulations due to the different true parameter values, and policies respond to that difference. If the temperature rises unexpectedly (due to the true value of the climate sensitivity being higher than the believed value), and no learning takes place, the planner attributes this only to higher weather shocks while anticipating lower future temperatures based on the initial beliefs. Therefore, the planner increases SGE by a relatively small amount. In contrast, under learning, when the temperature rises beliefs also rise, signalling to the planner that future temperatures will also rise. Therefore, the planner increases SGE by a larger amount with learning. The planner under learning bases SGE policy largely on beliefs because beliefs indicate likely paths of future temperatures. A similar argument holds for SGE effectiveness. When beliefs about SGE effectiveness rise, the planner increases SGE. However, without learning, even if SGE is effective the planner keeps the prior belief and does not increase SGE usage. Conversely, when the climate feedbacks are small and the temperature remains low, the planner without learning uses more SGE, anticipating future temperatures will evolve according to the prior distribution with a higher mean.

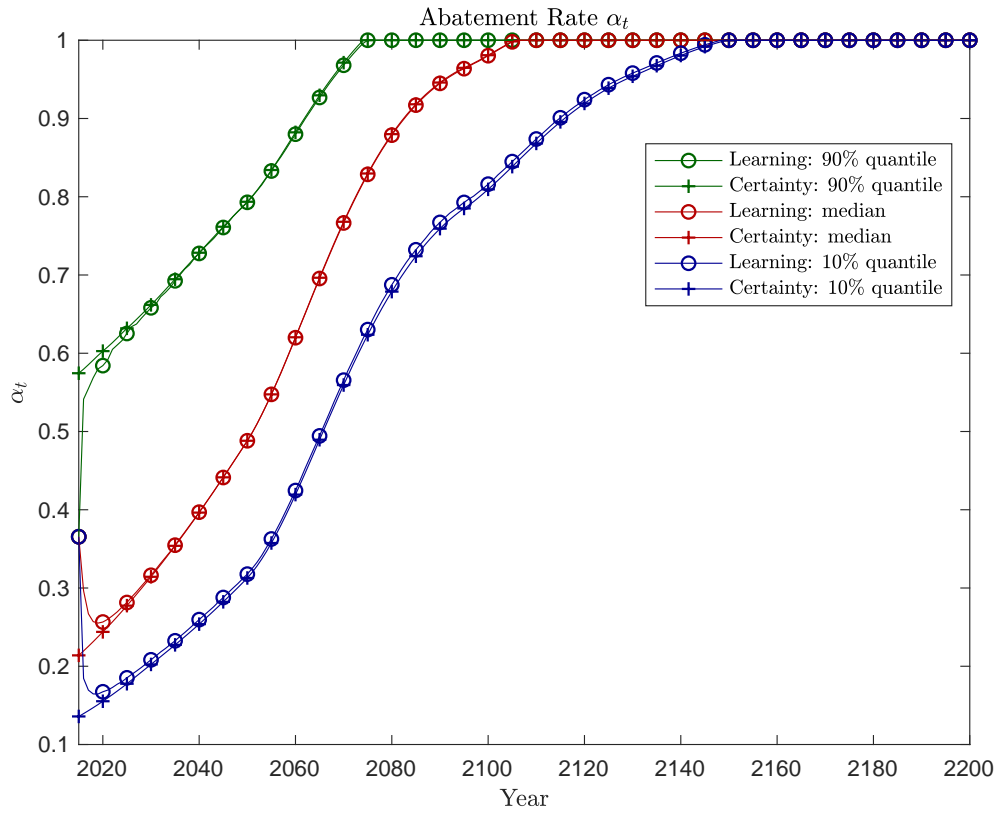


Figure 5: Abatement policy,  $\alpha_t$ , 10,000 simulations, learning and certainty.

Figure 5 compares optimal abatement policy under learning and under certainty. Like SGE, the initial median abatement policy is higher under learning, as a precaution against a potentially high climate sensitivity. Optimal abatement under learning is initially below the level that would occur if the climate sensitivity was known to be high for certain, however. The optimal policy under learning quickly converges to the certainty policy under all cases, since the residual uncertainty about SGE effectiveness is not as important for abatement policy as it is for SGE policy.

Figure 6 contrasts optimal abatement policy under learning with optimal abatement policy under uncertainty but no learning.

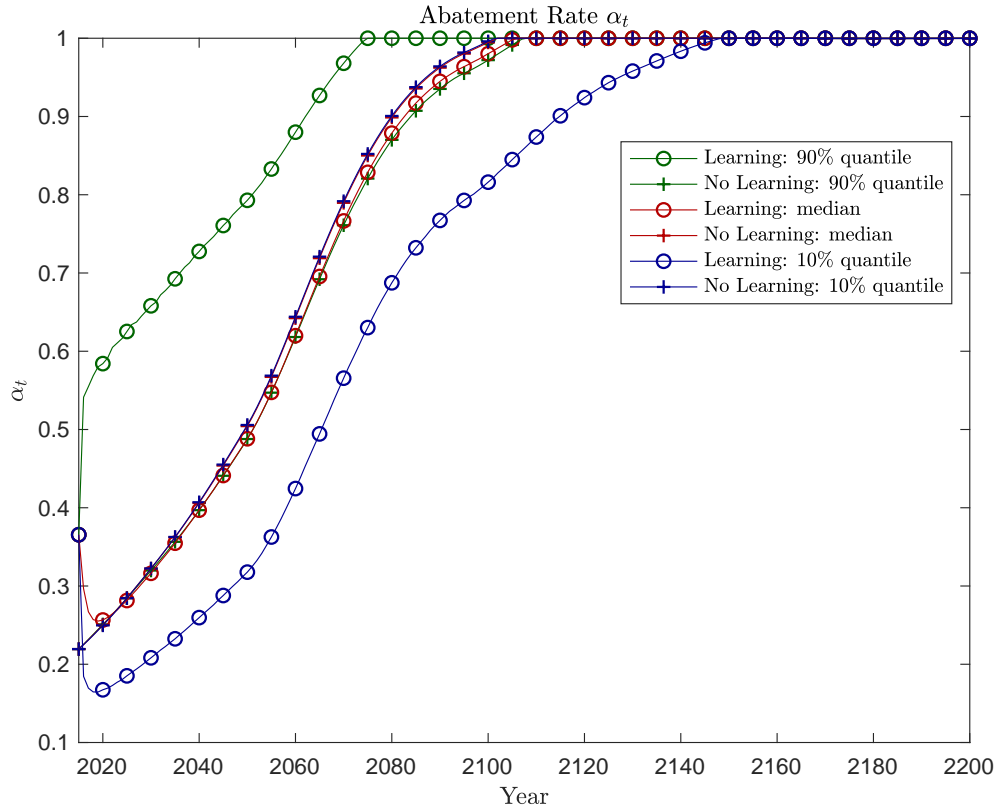


Figure 6: Abatement policy,  $\alpha_t$ , 10,000 simulations, learning and no learning.

In the case without learning, the planner's beliefs about the net feedback parameter and SGE effectiveness are unchanged through time and therefore, the policy response in both cases of high and low climate sensitivity hovers around the case with median climate sensitivity. In contrast, under learning the planner increases abatement when learning indicates the climate sensitivity is relatively high and the reverse.

Section 3 showed that experimentation with SGE slowed learning about both SGE effectiveness and climate sensitivity, given the 2015 initial conditions. However, the thresholds  $I_1$  and  $I_2$ , which determine whether or not SGE speeds learning, evolve over time. A natural question is whether or not optimal SGE ever exceeds  $I_1$  or  $I_2$ . If so, for these time periods SGE would speed learning about SGE effectiveness and the climate sensitivity, respectively. Optimal SGE would then have an information benefit from experimentation, rather than an information cost. Figure 7 investigates this issue by comparing the mean of  $I_1$  over time (the mean of  $I_2$  remains far above one for all  $t$ ) with the mean of optimal SGE. Though  $I_1$  declines over time, it is always greater than SGE deployment  $g$ .

The slowing of learning caused by SGE creates a disincentive for SGE use throughout the simulations, not just at the initial conditions.

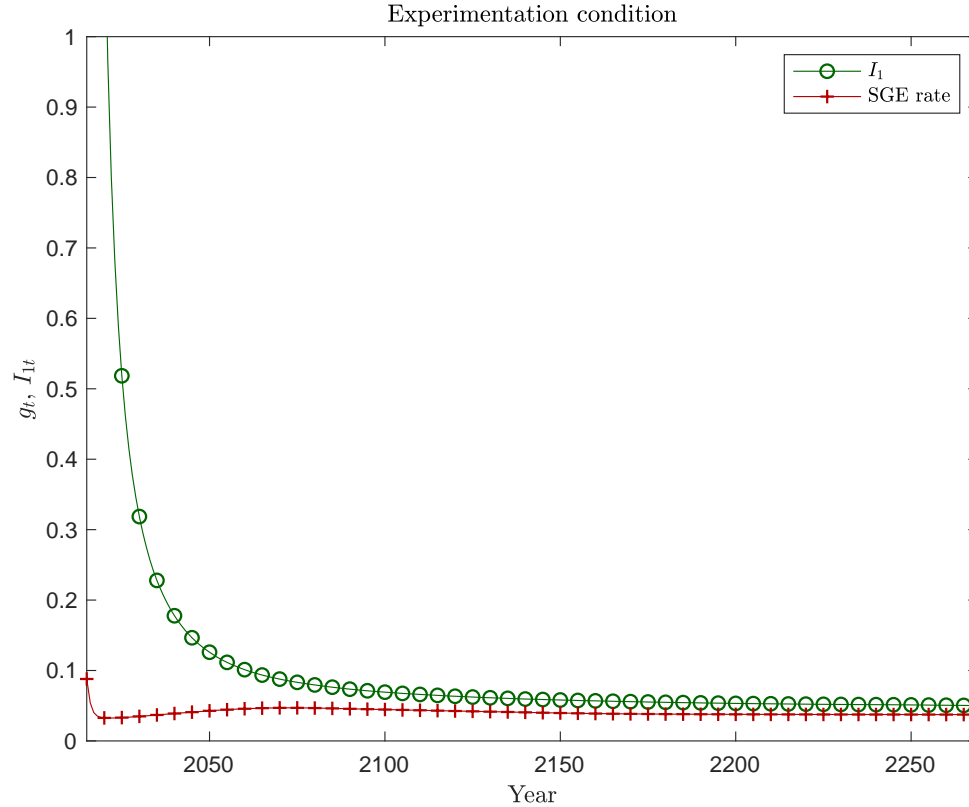


Figure 7: Threshold for SGE to speed learning about SGE effectiveness,  $I_{1t}$ , mean 10,000 simulations.

## 5 Conclusion

We present a model of optimal climate policy that includes the possibility of using solar geoengineering (SGE) to reduce temperatures. The model allows for uncertainty and endogenous learning over both climate sensitivity (the effect of carbon on temperature) and the effectiveness of SGE (the effect of SGE deployment on temperature). It allows for two policy variables – abatement and SGE – both of which affect the rate of learning about those uncertain parameters, creating a potential motivation to experiment with either policy to reduce uncertainty. However, we find that any reasonable level of SGE implementation actually slows learning. Since SGE has an uncertain effect on the climate, use of SGE essentially adds noise to the climate system. With SGE, the planner must

---

consider whether a warmer-than-expected year was the result of a random weather shock, a higher than expected climate sensitivity, or a lower than expected SGE effectiveness. Without SGE, only the first two of these possibilities exist and so learning evolves more quickly. Hence, given current conditions, no information justification exists for experimentation with SGE. Further, over time the information loss of using SGE continues, consistently reducing SGE usage.

Theoretically, we decompose the effect of SGE on learning into a signal strength effect and a noise amplification effect. The signal strength effect shows that small-scale SGE implementation reduces the magnitude of the temperature change and thus makes the temperature signal harder to observe amidst the noisy weather shocks. However, with large-scale SGE implementation, the planner expects to see a large change in temperature. Since a weather shock is unlikely to cause a large change in temperature, more information will be gained. Furthermore, any use of an uncertain SGE technology adds noise to the climate system, making learning over climate sensitivity more difficult; we call this the noise amplification effect.

Our numerical results show that SGE deployment is highly sensitive to beliefs about climate sensitivity and SGE effectiveness. Although SGE usage is generally low, it is substantially higher when beliefs indicate that climate change is likely to be severe and that SGE is effective at reducing temperature. Because the costs of both abatement and SGE are convex, some small amount of SGE is always optimal, as it is less costly than using only abatement.

Our model contains several simplifying assumptions that can be relaxed in extensions. We use the simplified version of DICE from Traeger (2014), and DICE itself is a relatively parsimonious integrated assessment model. Optimal policy is defined solely based on net discounted utility for the aggregate representative economy; our model does not incorporate any heterogeneity (e.g. by income, region) and does not consider equity criteria. Our model has endogenous learning over two uncertainties, but other parameters could also be modeled as uncertain, for example, SGE damages.

The findings are relevant for policymakers who may seek to deploy SGE both to immediately reduce temperatures and to learn more about SGE and the climate system. Our calibrated parameters based on volcanic eruptions, uncertain effectiveness, and loss of information suggest that SGE is less useful than previously thought, although some SGE is part of the optimal policy toolkit, especially if the planner learns the climate sensitivity is higher than expected.

## References

- Anna Lou Abatayo, Valentina Bosetti, Marco Casari, Riccardo Ghidoni, and Massimo Tavoni. Solar Geoengineering May Lead to Excessive Cooling and High Strategic Uncertainty. *Proceedings of the National Academy of Sciences*, 2020.
- J.E. Bickel and S. Agrawal. Reexamining the Economics of Aerosol Geoengineering. *Climatic Change*, 119(3-4):993–1006, 2013.
- J.E. Bickel and Lee Lane. An Analysis of Climate Engineering as a Response to Climate Change. Copenhagen Consensus Center Report, 40., 2009.
- Calum Brown, Peter Alexander, Almut Arneth, Ian Holman, and Mark Rounsevell. Achievement of Paris Climate Goals Unlikely Due to Time Lags in the Land System. *Nature Climate Change*, 9(3):203–208, 2019.
- Henrique de Oliveira. Blackwell’s Informativeness Theorem Using Diagrams. *Games and Economic Behavior*, 109:126–131, 2018.
- Simon Driscoll, Alessio Bozzo, Lesley J. Gray, Alan Robock, and Georgiy Stenchikov. Coupled Model Intercomparison Project 5 (CMIP5) Simulations of Climate Following Volcanic Eruptions. *Journal of Geophysical Research: Atmospheres*, 117(D17), 2012.
- Johannes Emmerling and Massimo Tavoni. Climate Engineering and Abatement: A ‘Flat’ Relationship Under Uncertainty. *Environmental and Resource Economics*, 69(2):395–415, 2018.
- Luke Fitzpatrick and David L. Kelly. Probabilistic Stabilization Targets. *Journal of the Association of Environmental and Resource Economists*, 4(2):611–57, June 2017.
- Jane A Flegal, Anna-Maria Hubert, David R Morrow, and Juan B Moreno-Cruz. Solar Geoengineering: Social Science, Legal, Ethical, and Economic Frameworks. *Annual Review of Environment and Resources*, 44:399–423, 2019.
- M. Goes, Nancy Tuana, and Klaus Keller. The Economics (or Lack Thereof) of Aerosol Geoengineering. *Climatic Change*, 109(3-4):719–744, 2011.
- K. Gramstad and S. Tjøotta. Climate Engineering: Cost Benefit and Beyond. University of Bergen, Department of Economics, No 05/10, 2010.

- 
- Patricia Heckendorn, Debra Weisenstein, Stephen Fueglistaler, Beiping P. Luo, Eugene Rozanov, M. Schraner, Larry W. Thomason, and Thomas Peter. The Impact of Geoengineering Aerosols on Stratospheric Temperature and Ozone. *Environmental Research Letters*, 4(4):045108, 2009.
- Koen G Helwegen, Claudia E Wieners, Jason E Frank, and Henk A Dijkstra. Complementing CO<sub>2</sub> Emission Reduction by Solar Radiation Management Might Strongly Enhance Future Welfare. *Earth System Dynamics*, 10(3):453–472, 2019.
- Garth Heutel, Juan Moreno-Cruz, and Katharine Ricke. Climate Engineering Economics. *Annual Review of Resource Economics*, 8:99–118, 2016a.
- Garth Heutel, Juan Moreno-Cruz, and Soheil Shayegh. Climate Tipping Points and Solar Geoengineering. *Journal of Economic Behavior and Organization*, 132:19–45, 2016b.
- Garth Heutel, Juan Moreno-Cruz, and Soheil Shayegh. Solar Geoengineering, Uncertainty, and the Price of Carbon. *Journal of Environmental Economics and Management*, 87:24–41, 2018.
- In Chang Hwang, Frédéric Reynès, and Richard SJ Tol. The Effect of Learning on Climate Policy under Fat-Tailed Risk. *Resource and Energy Economics*, 48:1–18, 2017.
- In Chang Hwang, Richard SJ Tol, and Marjan W Hofkes. Active Learning and Optimal Climate Policy. *Environmental and Resource Economics*, 73(4):1237–1264, 2019.
- Svenn Jensen and C.P. Traeger. Optimally Climate Sensitive Policy Under Uncertainty and Learning. Department of Agricultural & Resource Economics, UC Berkeley, 2013.
- David W Keith, Riley Duren, and Douglas G. MacMartin. Field Experiments on Solar Geoengineering: Report of a Workshop Exploring a Representative Research Portfolio. *Philosophical Transactions of the Royal Society A: Mathematical, Physical and Engineering Sciences*, 372(2031):20140175, 2014.
- David P Keller, Ellias Y Feng, and Andreas Oeschles. Potential Climate Engineering Effectiveness and Side Effects During a High Carbon Dioxide-Emission Scenario. *Nature Communications*, 5:3304, 2014.
- David L. Kelly and Charles D. Kolstad. Bayesian Learning, Growth, and Pollution. *Journal of Economic Dynamics and Control*, 23(4):491–518, 1999.



- 
- David L. Kelly and Zhuo Tan. Learning and Climate Feedbacks: Optimal Climate Insurance and Fat Tails. *Journal of Environmental Economics and Management*, 72:98–122, 2015.
- Gernot Klepper and Wilfried Rickels. Climate Engineering: Economic Considerations and Research Challenges. *Review of Environmental Economics and Policy*, 8(2):270–289, 2014.
- Ben Kravitz and Douglas G MacMartin. Uncertainty and the Basis for Confidence in Solar Geoengineering Research. *Nature Reviews Earth & Environment*, 1(1):64–75, 2020.
- Ben Kravitz, Douglas G MacMartin, Simone Tilmes, Jadwiga H Richter, Michael J Mills, Wei Cheng, Katherine Dagon, Anne S Glanville, Jean-Francois Lamarque, Isla R Simpson, Joseph Tribbia, and Francis Vitt. Comparing Surface and Stratospheric Impacts of Geoengineering with Different SO<sub>2</sub> Injection Strategies. *Journal of Geophysical Research: Atmospheres*, 124(14):7900–7918, 2019.
- Roman Krzysztofowicz. Markovian Forecast Processes. *Journal of the American Statistical Association*, 82(397):31–37, 1987.
- Jacob LaRiviere, David Kling, James N. Sanchirico, Charles Sims, and Michael Springborn. The Treatment of Uncertainty and Learning in the Economics of Natural Resource and Environmental Management. *Review of Environmental Economics and Policy*, 12(1):92–112, 2018.
- Andrew J. Leach. The Climate Change Learning Curve. *Journal of Economic Dynamics and Control*, 31(5):1728–1752, 2007.
- Derek Lemoine and Ivan Rudik. Managing Climate Change under Uncertainty: Recursive Integrated Assessment at an Inflection point. *Annual Review of Resource Economics*, 9:117–142, 2017.
- Derek Lemoine and Christian Traeger. Watch Your Step: Optimal Policy in a Tipping Climate. *American Economic Journal: Economic Policy*, 6(1):137–166, 2014.
- Juan Moreno-Cruz and David Keith. Climate Policy under Uncertainty: a Case for Solar Geoengineering. *Climatic Change*, 121:431–444, 2013.
- National Research Council, et. al. *Climate Intervention: Reflecting Sunlight to Cool Earth*. National Academies Press, 2015.
- William D. Nordhaus. Revisiting the Social Cost of Carbon. *Proceedings of the National Academy of Sciences*, 114(7):1518–1523, January 2016.

- 
- AV Pastor, DCS Vieira, FH Soudijn, and OY Edelenbosch. How Uncertainties are Tackled in Multi-disciplinary Science? A Review of Integrated Assessments under Global Change. *Catena*, 186: 104305, 2020.
- Jonathan Proctor, Solomon Hsian, Jennifer Burney, Marshall Burke, and Wolfram Schlenker. Estimating Global Agricultural Effects of Geoengineering Using Volcanic Eruptions. *Nature*, 560 (7719):480–483, 2018.
- Adrian E Raftery, Alec Zimmer, Dargan MW Frierson, Richard Startz, and Peiran Liu. Less Than 2 C Warming by 2100 Unlikely. *Nature Climate Change*, 7(9):637, 2017.
- Venkatachalam Ramaswamy, W Collins, J Haywood, J Lean, N Mahowald, G Myhre, V Naik, KP Shine, B Soden, G Stenchikov, and T Storelvmo. Radiative Forcing of Climate: the Historical Evolution of the Radiative Forcing Concept, the Forcing Agents and their Quantification, and Applications. *Meteorological Monographs*, 59:14.1–14.101, 2018.
- Katharine L. Ricke. *Characterizing Impacts and Implications of Proposals for Solar Radiation Management, a Form of Climate Engineering*. PhD thesis, Carnegie Mellon University, 2011.
- Gerard H. Roe and Marcia B. Baker. Why is Climate Sensitivity so Unpredictable? *Science*, 318 (5850):629–32, 2007.
- Soheil Shayegh and Valerie M Thomas. Adaptive Stochastic Integrated Assessment Modeling of Optimal Greenhouse Gas Emission Reductions. *Climatic Change*, 128(1-2):1–15, 2015.
- Christian Traeger. A 4-stated DICE: Quantitatively Addressing Uncertainty Effects in Climate Change. *Environmental and Resource Economics*, 59:1–37, 2014.
- Martin L. Weitzman. On Modeling and Interpreting the Economics of Catastrophic Climate Change. *Review of Economics and Statistics*, 91:1–19, 2009.

# Appendix

## A Details of Numerical Model

### A.1 Optimization Problem

The full model is the optimization problem, plus the equations governing the evolution of the exogenous variables. Exogenous variables depend only on the time state and are denoted as functions of  $t$ . All endogenous state and control variables vary over time. We suppress the  $t$  subscript on all current state and control variables, and primes denote next-period values. The objective is:

$$v(S) = \max_{K', g, \alpha} \left\{ L(t) \frac{\left(\frac{C}{L(t)}\right)^{1-\omega} - 1}{1-\omega} + \exp(-\delta_u t) \int_{-\infty}^{\infty} v(S'(H')) \Phi[H', \mu_H, P_H^{-1}] dH' \right\}. \quad (\text{A.1})$$

The planner chooses  $g$  and  $\alpha$  along with savings, defining next period's capital stock  $K'$ . Here  $L(t)$  is the exogenously-determined population,  $\omega$  is the utility curvature parameter, and  $\delta_u$  is the pure rate of time preference. Here also  $\Phi$  is the normal density and  $S$  is a vector of state variables:

$$S = [K, T_{AT}, M, t, \mu, P], \quad (\text{A.2})$$

In equation (A.2), the state vector consists of the stock of capital,  $K$ ; the atmospheric temperature,  $T_{AT}$ ; the atmospheric stock of carbon,  $M$ ; and the time state  $t$ . The state vector also consists of five learning states:  $\mu$  is a 2-dimensional vector  $(\beta, \phi)$  and  $P$  is a matrix with 3 independent elements ( $P_1, P_2$ , and  $P_3$ ). Thus the state vector has 9 total dimensions.

The maximization is subject to the following equations:

$$Q = K^\gamma (A(t) L(t))^{1-\gamma}, \quad (\text{A.3})$$

$$Y = (1 - \Lambda - D) Q, \quad (\text{A.4})$$

$$C = Y + (1 - \delta_k) K - K'. \quad (\text{A.5})$$

Here equation (A.3) defines gross output. Equation (A.4) gives net output equal to gross output less total climate damages and abatement and SGE costs. Here  $D$  is damages as a fraction of

gross output and  $\Lambda$  are abatement and SGE costs as a fraction of gross output. Equation (A.5) defines consumption as net output less savings. Savings is next period's capital  $K'$  less capital net of depreciation,  $(1 - \delta_k)K$ . Damages are:

$$D = \pi_T T_{AT}^2 + \pi_m (M - M_{1750})^2 + \pi_g g^2. \quad (\text{A.6})$$

Climate change damages  $D$  are a function of atmospheric temperature  $T_{AT}$ , as in the original DICE model, but also of carbon  $M$ , reflecting the fact that SGE reduces temperature without reducing carbon stocks. Use of SGE also causes damage directly through the term  $\pi_g g^2$ .

Costs from abatement and SGE are both modeled as power functions of abatement and SGE intensities, respectively.

$$\Lambda = \theta_1 (t) \alpha^{\theta_2} + \theta_{GE} g^{\theta_3}, \quad (\text{A.7})$$

Emissions  $E$  are

$$E = \sigma (t) (1 - \alpha) (A (t) L (t))^{1-\gamma} + E_{LAND} (t). \quad (\text{A.8})$$

Emissions are a function of industrial emissions ( $\sigma (t) K^\gamma (A (t) L (t))^{1-\gamma}$ ) minus abatement, plus exogenous emissions from land use changes denoted by  $E_{LAND}$ .

The carbon cycle, radiative forcing, and temperature, and learning variables evolve as defined in Section 2. For completeness, the equations are repeated here:

$$M' = M_{1750} + (1 - \delta_m (t)) (M - M_{1750}) + E. \quad (\text{A.9})$$

$$F' = \left( \eta \log_2 \left[ \frac{M'}{M_{1750}} \right] + F_{EX} (t + 1) \right) (1 - \phi g), \quad (\text{A.10})$$

$$T'_{AT} = T_{AT} + \xi_1 \left\{ F' - \xi_2 T_{AT} - \xi_3 [T_{AT} - T_{LO}] (t) \right\} + \epsilon'. \quad (\text{A.11})$$

$$P' = P + \rho_\epsilon X X^{tr}, \quad (\text{A.12})$$

$$X = \begin{bmatrix} T_{AT} \\ -\hat{F}'g \end{bmatrix}, \quad (\text{A.13})$$

$$\mu' = (P')^{-1} (P\mu + \rho_\epsilon X H'), \quad (\text{A.14})$$

$$\mu = \begin{bmatrix} \beta \\ \phi \end{bmatrix}, \quad (\text{A.15})$$

$$t' = t + 1. \quad (\text{A.16})$$

$$\mu_H = X^{tr} \mu, \quad (\text{A.17})$$

$$\text{var}_H = X^{tr} P^{-1} X + \rho_\epsilon^{-1} \quad (\text{A.18})$$

The exogenous variables evolve according to:

$$L(t) = L(0) + (L(\infty) - L(0))(1 - \exp(-g_L t)) \quad (\text{A.19})$$

$$A(t) = A(0) \exp \left[ g_A(0) \frac{(1 - \exp(-\delta_A))}{\delta_A} \right] \quad (\text{A.20})$$

$$g_A(t) = \log \left[ \frac{A(t+1)}{A(t)} \right] \quad (\text{A.21})$$

$$g_L(t) = \log \left[ \frac{L(t+1)}{L(t)} \right] \quad (\text{A.22})$$

$$\sigma(t) = \sigma(0) \exp \left[ g_\sigma(0) \frac{(1 - \exp(-\delta_\sigma))}{\delta_\sigma} \right] \quad (\text{A.23})$$

$$\theta_1(t) = \sigma(t) \frac{\theta_p}{\theta_2} \exp[-\delta_p t] \quad (\text{A.24})$$

$$E_{LAND}(t) = E_{LAND}(0) \exp(-\delta_{LAND} t) \quad (\text{A.25})$$

$$\delta_m(t) = \delta_m(\infty) + (\delta_m(0) - \delta_m(\infty)) \exp(-\delta_m^* t), \quad (\text{A.26})$$

$$EF(t) = EF(0) + (EF(\infty) - EF(0)) \min \left( \frac{t}{85}, 1 \right) \quad (\text{A.27})$$

$$[T_{AT} - T_{LO}](t) = \max \{ \delta_{T,1} + \delta_{T,2} t + \delta_{T,3} t^2, 0 \} \quad (\text{A.28})$$

Equations (A.19)-(A.28) are continuous-time approximations of the exogenous equations in DICE provided by Traeger (2014).

## A.2 Normalization

We next normalize the model and introduce several changes of variables that make the analysis more convenient. Let  $k \equiv \frac{K}{AL}$  denote capital per productivity-adjusted person and the same for  $c$ , and let  $m \equiv \frac{M}{M_{1750}}$ . In addition, let:

$$gr_{AL}(t) = \frac{L(t+1)A(t+1)}{L(t)A(t)}, \quad (\text{A.29})$$

$$gr_A(t) = \frac{A(t+1)}{A(t)}, \quad gr_L(t) = \frac{L(t+1)}{L(t)}, \quad (\text{A.30})$$

$$r(t) = \exp \left[ -\delta_u + \log \left( gr_A(t)^{1-\omega} \right) + \log (gr_L(t)) \right], \quad (\text{A.31})$$

where  $gr$  denotes the gross growth rates and the levels of the exogenous variables are defined in equations (A.19)-(A.28). Let  $\hat{\pi}_m = \pi_m M_{1750}^2$ ,  $\sigma AL(t) = \sigma(t)A(t)L(t)$ , and  $\psi = 1/M_{1750}$ .

Next, we replace  $H'$  by a standard normal random variable. Let:

$$z' = \frac{H' - \mu_H}{\text{var}_H^{\frac{1}{2}}}, \quad (\text{A.32})$$

$$H' = \mu_H + \text{var}_H^{\frac{1}{2}} z', \quad (\text{A.33})$$

$$dH' = \text{var}_H^{\frac{1}{2}} dz'. \quad (\text{A.34})$$

In the above set up, the time state and the precision variables are unbounded (see equation A.12). The computational algorithm requires each state variable to be on a bounded domain. We can replace the time state with a bounded function:

$$\hat{t} = 1 - \exp(-\tau t). \quad (\text{A.35})$$

Further, we can replace the precision  $P$  with the variance:

$$W = P^{-1} \equiv \begin{bmatrix} W_1 & W_2 \\ W_2 & W_3 \end{bmatrix}. \quad (\text{A.36})$$

To simplify the model, we first integrate via substitution using (A.32):

$$\begin{aligned}
& \int_{-\infty}^{\infty} v(S'(H')) \Phi[H', \mu_H, \text{var}_H] dH' \\
&= \int_{-\infty}^{\infty} v\left(S'\left(\mu_H + \text{var}_H^{\frac{1}{2}} z'\right)\right) \Phi\left[\mu_H + \text{var}_H^{\frac{1}{2}} z', \mu_H, \text{var}_H\right] \text{var}_H^{\frac{1}{2}} dz' \\
&= \int_{-\infty}^{\infty} v\left(S'\left(\mu_H + \text{var}_H^{\frac{1}{2}} z'\right)\right) \Phi[z', 0, 1] dz',
\end{aligned} \tag{A.37}$$

where the last equality follows from the definition of the normal distribution. Hence the maximization problem is unchanged by replacing  $H'$  with  $\mu_H + \text{var}_H^{\frac{1}{2}} z'$  in the constraints and integrating using the standard normal distribution.

Next, since by definition,  $W = P^{-1}$ ,  $(P')^{-1} = W'$ . Thus (A.12) becomes:

$$(W')^{-1} = W^{-1} + \rho_\epsilon X X^{tr}, \tag{A.38}$$

$$W' = (W^{-1} + \rho_\epsilon X X^{tr})^{-1}, \tag{A.39}$$

and similarly for the other constraints which are functions of the precision.

Finally, the normalization replacing the aggregate economic variables with per-productivity unit variables is identical to Traeger (2014). After replacing  $M$  with  $m/\psi$ , the model reduces to:

$$v(s) = \max_{k', g, \alpha} \left\{ \frac{c^{1-\omega} - 1}{1-\omega} + r(t) \int_{-\infty}^{\infty} v(s'(z')) \Phi[z', 0, 1] dz' \right\}. \tag{A.40}$$

Subject to:

$$s = [k, T_{AT}, m, \hat{t}, \mu, W], \tag{A.41}$$

$$c = (1 - \Lambda - D) k^\gamma + (1 - \delta_k) k - gr_{AL}(t) k', \tag{A.42}$$

$$D = \pi_T T_{AT}^2 + \hat{\pi}_m (m - 1)^2 + \pi_g g^2, \tag{A.43}$$

$$\Lambda = \theta_1(t) \alpha^{\theta_2} + \theta_{GE} g^{\theta_3}, \tag{A.44}$$

$$E = \sigma AL(t) (1 - \alpha) k^\gamma + E_{LAND}(t), \tag{A.45}$$

$$m' = 1 + (1 - \delta_m(t)) (m - 1) + \psi E, \tag{A.46}$$

$$\hat{F}' = \xi_1 (\eta \log_2 [m'] + F_{EX}(t')), \tag{A.47}$$

$$T'_{AT} = \hat{F}' - \xi_1 \xi_3 (T_{AT} - T_{LO})(t) + \mu_H + \text{var}_{\frac{1}{2}H} z', \quad (\text{A.48})$$

$$W' = (W^{-1} + \rho_\epsilon X X^{tr})^{-1}, \quad (\text{A.49})$$

$$X = \begin{bmatrix} T_{AT} \\ -\hat{F}'g \end{bmatrix}, \quad (\text{A.50})$$

$$\mu' = W' \left( W^{-1} \mu + \rho_\epsilon X \left( \mu_H + \text{var}_{\frac{1}{2}H} z' \right) \right), \quad (\text{A.51})$$

$$\mu = \begin{bmatrix} \beta \\ \phi \end{bmatrix}, \quad (\text{A.52})$$

$$t = -\frac{1}{\tau} \log(1 - \hat{t}) \quad (\text{A.53})$$

$$\hat{t}' = 1 - (1 - \hat{t}) \exp(-\tau), \quad (\text{A.54})$$

$$\mu_H = X^{tr} \mu, \quad (\text{A.55})$$

$$\text{var}_H = X^{tr} W X + \rho_\epsilon^{-1}, \quad (\text{A.56})$$

plus the exogenous equations (A.19)-(A.28).

Note that uncertainty enters into the original model through the distribution for  $H'$ , in equation (17). In the normalized model, uncertainty enters directly into the temperature equation (A.48).

## B Proofs

### B.1 Proof of Proposition 1

We first show that each element of  $W'$  is positive. Let  $W$  satisfy the assumptions of the proposition, so that  $W$  is positive definite,  $W_1 W_3 > W_2^2$ . Then:

$$X^{tr} W X > X_1^2 W_1 + 2X_1 X_2 W_2 + X_2^2 \frac{W_2^2}{W_1} = \frac{1}{W_1} (X_1 W_2 + X_2 W_1)^2 > 0, \quad (\text{B.1})$$

where the first inequality follows from  $W$  being positive definite, and the second from  $W_3 > 0$  by assumption. Thus, from equation (21),  $W'_1 > 0$ ,  $W'_3 > 0$  and since  $X_2 < 0$ ,  $W'_2 > 0$ .



Next, we show that  $W'$  is positive definite. Note that:

$$\begin{aligned} |W'| &= \left( \frac{1}{1 + \rho_\epsilon X^{tr} W X} \right)^2 \left[ (W_1 + \rho_\epsilon |W| X_2^2) (W_3 + \rho_\epsilon |W| X_1^2) - (W_2 - \rho_\epsilon |W| X_1 X_2)^2 \right] \\ &= \frac{|W|}{1 + \rho_\epsilon X^{tr} W X}, \end{aligned} \quad (\text{B.2})$$

which is positive as shown in (B.1). Therefore, by induction the elements of  $W$  remain non-negative and  $W$  remains positive definite for all  $t$ .

Next, we bound  $W'$  from above. Consider first  $W_1$ . We have  $W_1' < W_1$  if and only if:

$$\frac{W_1 + \rho_\epsilon |W| X_2^2}{1 + \rho_\epsilon X^{tr} W X} < W_1, \quad (\text{B.3})$$

which simplifies to:

$$0 < (W_1 X_1 + W_2 X_2)^2. \quad (\text{B.4})$$

Thus,  $W_1' < W_1$  and by induction  $W_{1,t} < W_{1,0}$  for all  $t$ . The same result holds for  $W_3$  by an analogous argument. For  $W_2$ , since  $W$  remains positive definite, we have:

$$W_2^2 < W_1 W_3. \quad (\text{B.5})$$

Since, as shown above,  $W_1$  and  $W_3$  are bounded by their initial values:

$$W_2 < (W_1 W_3)^{\frac{1}{2}} < (W_{1,0} W_{3,0})^{\frac{1}{2}} \quad \forall t. \quad (\text{B.6})$$

Hence  $W_{2,t}$  is also bounded for all  $t$ .

## B.2 Proof of Proposition 2

First we show  $I_1 < I' < I_2$ . By definition,  $I' < I_2$  if and only if:

$$I' \equiv \frac{T}{\hat{F}'} \frac{W_2' W_2 + W_3' W_1}{W_2' W_3 + W_3' W_2} < I_2 \equiv \frac{T}{\hat{F}'} \frac{W_1}{W_2}. \quad (\text{B.7})$$

Multiplying out the terms yields:

$$0 < W_2' |W|, \quad (\text{B.8})$$

which is satisfied for all  $t$  from Proposition 1. Further,  $I_1 < I'$  if and only if:

$$I_1 \equiv \frac{T}{\hat{F}'} \frac{W_2}{W_3} < I' \equiv \frac{T}{\hat{F}'} \frac{W_2'W_2 + W_3'W_1}{W_2'W_3 + W_3'W_2}. \quad (\text{B.9})$$

Multiplying out the terms results in:

$$0 < W_3' |W|, \quad (\text{B.10})$$

which is satisfied for all  $t$  from Proposition 1.

Next, we want to find the effect of SGE  $g$  in the current period on uncertainty  $W'$  next period:

$\frac{\partial W'}{\partial g}$ . Since  $W'$  is a function of both  $X_1 = T_{AT}$  and  $X_2 = -\hat{F}'g$ ,

$$\frac{\partial W'}{\partial g} = \frac{\partial W'}{\partial X_1} \frac{\partial X_1}{\partial g} + \frac{\partial W'}{\partial X_2} \frac{\partial X_2}{\partial g} \quad (\text{B.11})$$

Since both current period  $X_1 = T_{AT}$  and  $\hat{F}'$  are unaffected by current-period SGE  $g$ ,  $\frac{\partial X_1}{\partial g} = 0$  and  $\frac{\partial X_2}{\partial g} = -\hat{F}'$ . So,

$$\frac{\partial W'}{\partial g} = \frac{\partial W'}{\partial X_2} \cdot (-\hat{F}'). \quad (\text{B.12})$$

It follows that  $\frac{\partial W'}{\partial g} < 0$  if and only if  $\frac{\partial W'}{\partial X_2} > 0$ .

The derivative of  $W'$  with respect to  $X_2$  from equation (21) is:

$$\begin{aligned} \frac{\partial W'}{\partial X_2} &= \frac{-2\rho_\epsilon (W_2X_1 + W_3X_2)}{(1 + \rho_\epsilon X^{tr}WX)^2} \begin{bmatrix} W_1 + \rho_\epsilon |W| X_2^2 & W_2 - \rho_\epsilon |W| X_1X_2 \\ W_2 - \rho_\epsilon |W| X_1X_2 & W_3 + \rho_\epsilon |W| X_1^2 \end{bmatrix} \\ &+ \frac{\rho_\epsilon |W|}{(1 + \rho_\epsilon X^{tr}WX)} \begin{bmatrix} 2X_2 & -X_1 \\ -X_1 & 0 \end{bmatrix} \end{aligned} \quad (\text{B.13})$$

$$= \frac{-\rho_\epsilon}{(1 + \rho_\epsilon X^{tr}WX)^2} \begin{bmatrix} A_w & B_w \\ B_w & C_w \end{bmatrix}, \quad (\text{B.14})$$

where:

$$A_w = 2(W_2X_1 + W_3X_2)(W_1 + \rho_\epsilon |W| X_2^2) - 2|W| X_2 (1 + \rho_\epsilon X^{tr}WX), \quad (\text{B.15})$$

$$= 2\{W_1W_2X_1 + W_2^2X_2 - \rho_\epsilon |W| X_2X_1 (W_1X_1 + W_2X_2)\}, \quad (\text{B.16})$$

$$= 2(W_2 - \rho_\epsilon |W| X_2X_1)(W_1X_1 + W_2X_2), \quad (\text{B.17})$$

$$A_w = 2W_2' (1 + \rho_\epsilon X^{tr} W X) (W_1 X_1 + W_2 X_2), \quad (\text{B.18})$$

$$B_w = 2(W_2 X_1 + W_3 X_2) (W_2 - \rho_\epsilon |W| X_1 X_2) + |W| X_1 (1 + \rho_\epsilon X^{tr} W X), \quad (\text{B.19})$$

$$= W_2^2 X_1 + 2W_2 W_3 X_2 + W_1 W_3 X_1 + \rho_\epsilon |W| X_1 (X_1^2 W_1 - X_2 W_3), \quad (\text{B.20})$$

$$= W_2 (W_2 X_1 + W_3 X_2) + W_3 (W_1 X_1 + W_2 X_2) + \rho_\epsilon |W| X_1 (-X_2 (W_2 X_1 + W_3 X_2) + X_1 (W_1 X_1 + W_2 X_2)), \quad (\text{B.21})$$

$$B_w = \left[ W_2' (W_2 X_1 + W_3 X_2) + W_3' (W_1 X_1 + W_2 X_2) \right] (1 + \rho_\epsilon X^{tr} W X), \quad (\text{B.22})$$

$$C_w = 2(W_2 X_1 + W_3 X_2) (W_3 + \rho_\epsilon |W| X_1^2) \quad (\text{B.23})$$

$$C_w = 2(W_2 X_1 + W_3 X_2) W_3' (1 + \rho_\epsilon X^{tr} W X). \quad (\text{B.24})$$

Combining equations (B.14), (B.18), (B.22), and (B.24) reveals that:

$$\frac{\partial W'}{\partial X_2} = \frac{-\rho_\epsilon}{(1 + \rho_\epsilon X^{tr} W X)} \begin{bmatrix} 2\hat{W}_A W_2' & \hat{W}_A W_3' + \hat{W}_B W_2' \\ \hat{W}_A W_3' + \hat{W}_B W_2' & 2\hat{W}_B W_3' \end{bmatrix} \quad (\text{B.25})$$

$$\hat{W}_A \equiv W_1 X_1 + W_2 X_2$$

$$\hat{W}_B \equiv W_2 X_1 + W_3 X_2$$

Next, Proposition 1 shows that  $W_i' > 0$  for  $i = 1, 2, 3$  and all  $t$ . Hence:

$$\frac{\partial W_1'}{\partial X_2} > 0 \iff \hat{W}_A < 0 \iff g > \frac{W_1}{W_2} \cdot \frac{T}{\hat{F}'} = I_2. \quad (\text{B.26})$$

$$\frac{\partial W_2'}{\partial X_2} > 0 \iff \hat{W}_A W_3' + \hat{W}_B W_2' < 0 \iff g > \frac{W_2' W_2 + W_3' W_1}{W_2' W_3 + W_3' W_2} \cdot \frac{T}{\hat{F}'} = I'. \quad (\text{B.27})$$

$$\frac{\partial W_3'}{\partial X_2} > 0 \iff \hat{W}_B < 0 \iff g > \frac{W_2}{W_3} \cdot \frac{T}{\hat{F}'} = I_1. \quad (\text{B.28})$$

Given (B.26)-(B.28) and  $I_1 < I' < I_2$ , and the fact that  $\frac{\partial W'}{\partial g} < 0$  if and only if  $\frac{\partial W'}{\partial X_2} > 0$ , the sign of the derivatives in each region is immediate.<sup>30</sup>

<sup>30</sup>Strictly speaking,  $B_w$  is a quadratic function of  $X_2$  since  $W_2'$  depends on  $X_2$ . However, one can show that exactly one root exists for  $B_w$  over the domain  $X_2 < 0$ . Therefore, the given condition (B.27) remains valid.

### B.3 Proof of Proposition 3

To evaluate the derivative of  $W'$  with respect to  $\alpha$ , note that

$$\frac{\partial W'}{\partial \alpha} = \frac{\partial W'}{\partial X_1} \frac{\partial X_1}{\partial \alpha} + \frac{\partial W'}{\partial X_2} \frac{\partial X_2}{\partial \alpha} \quad (\text{B.29})$$

Note that  $X_1 = T_{AT}$  is unaffected by current abatement  $\alpha$ . Further,  $X_2 = -\hat{F}'g$ , and though  $g$  is unaffected by  $\alpha$ ,  $\hat{F}'$  is. In fact, since  $\hat{F}' = \xi_1 \left( \eta \log_2 \left[ \frac{M'}{M_{1750}} \right] + F_{EX}(t+1) \right)$ , it follows that  $\frac{\partial \hat{F}'}{\partial \alpha} = \xi_1 \eta \frac{1}{M' \ln 2} \frac{\partial M'}{\partial \alpha} < 0$ , since  $\frac{\partial M'}{\partial \alpha} = -\sigma(t)Q$ . Thus,  $\frac{\partial X_2}{\partial \alpha} < 0$ , so  $\frac{\partial W'}{\partial \alpha}$  has the same sign of  $\frac{\partial W'}{\partial X_2}$ .

Then, all the steps of the proof of Proposition 2 follow, generating the same conditions but with opposite sign as Proposition 2 (whenever  $\frac{\partial W'}{\partial g} < 0$ ,  $\frac{\partial W'}{\partial \alpha} > 0$ ).

### B.4 Proof of Proposition 4

For Blackwell Informativeness, we first note that problem (A.40) can be written with  $T'$  as the random variable:

$$v(s) = \max_{k', g, \alpha} \left\{ \frac{c^{1-\omega} - 1}{1 - \omega} + r(t) \int_{-\infty}^{\infty} v(s'(T')) \Phi[T', b_T + \mu_H, \text{var}_H] dT' \right\}. \quad (\text{B.30})$$

Here:

$$b_T = \hat{F}' - \xi_1 \xi_3 (T_{AT} - T_{LO})(t), \quad (\text{B.31})$$

and all other constraints are the same except (A.51), which becomes:

$$\mu' = W' (W^{-1} \mu + \rho_\epsilon X (T' - b_T)), \quad (\text{B.32})$$

From Blackwell's theorem, experiment  $g_2$  produces a distribution over  $T'$  which is more informative than experiment  $g_1$  if the signal of  $T'$  from experiment  $g_1$  can be found by garbling the signal from experiment  $g_2$ .<sup>31</sup> That is, experiment  $g_2$  is more Blackwell informative if there exists a

<sup>31</sup>See, for example, de Oliveira (2018).

distribution  $\Psi$  such that:<sup>32</sup>

$$\begin{aligned}\Phi(T'_1; \mu_1, \text{var}_1) &= \int_{-\infty}^{\infty} \Psi(T'_1|T'_2) \Phi(T'_2; \mu_2, \text{var}_2) dT'_2, \\ \mu_i &= b_T + \mu' (g_i)^{tr} X, \quad i = 1, 2, \\ \text{var}_i &= X^{tr} W' (g_i) X + \rho_\epsilon^{-1}, \quad i = 1, 2.\end{aligned}\tag{B.33}$$

That is, the experiment  $g_2$  is more informative if one can add additional randomness to (garble) the signal produced by experiment  $g_2$  and get the signal produced by experiment  $g_1$ . From Blackwell's theorem, if such a distribution  $\Psi$  can be found, then experiment two is a more accurate signal and produces higher utility, all other things equal.

We hypothesize that  $\Psi$  is a normal distribution:

$$\Psi(T'_1|T'_2) = \Phi(T'_1; A + BT'_2, \text{var}_\psi).\tag{B.34}$$

Here  $A$ ,  $B$ , and  $\text{var}_\psi$  are undetermined coefficients.

Given the guess, the right hand side of equation (B.33) integrates to:

$$\begin{aligned}r.h.s. &= (2\pi)^{-\frac{1}{2}} (\text{var}^*)^{-\frac{1}{2}} \exp\left\{-\frac{1}{2} \text{var}^* (T'_1 - \mu^*)^2\right\}, \\ \text{var}^* &= A^2 \text{var}_2 + \text{var}_\psi \\ \mu^* &= B + \mu_2 A\end{aligned}\tag{B.35}$$

Hence, given the guess, the right hand side integrates to the normal density:

$$r.h.s. = \Phi(T'_1; \mu^*, \text{var}^*)\tag{B.36}$$

Hence, the guess is verified by equating the mean and variance of the right hand side and left hand side of (B.33).

$$b_T + \mu' (g_1)^{tr} X = \mu^* = B + \left(b_T + \mu' (g_2)^{tr} X\right) A\tag{B.37}$$

<sup>32</sup>Here we essentially extend the argument of Krzysztofowicz (Krzysztofowicz, 1987) to multiple dimensions.

The undetermined coefficients are then set so that the means are equal for all  $X$ :

$$\begin{aligned} A &= \frac{\mu'(g_1)^{tr} X}{\mu'(g_2)^{tr} X} \\ B &= b_T \left( 1 - \frac{\mu'(g_1)^{tr} X}{\mu'(g_2)^{tr} X} \right). \end{aligned} \quad (\text{B.38})$$

Equating the variances results in:

$$\text{var}_1 = \text{var}^* = A^2 \text{var}_2 + \text{var}_\psi, \quad (\text{B.39})$$

$$\text{var}_\psi = X^{tr} W'(g_1) X + \rho_\epsilon^{-1} - (X^{tr} W'(g_2) X + \rho_\epsilon^{-1}) \left( \frac{\mu'(g_1)^{tr} X}{\mu'(g_2)^{tr} X} \right)^2. \quad (\text{B.40})$$

For  $\Psi$  to be a valid distribution, the variance must be positive. Therefore:

$$X^{tr} W'(g_1) X + \rho_\epsilon^{-1} - (X^{tr} W'(g_2) X + \rho_\epsilon^{-1}) \left( \frac{\mu'(g_1)^{tr} X}{\mu'(g_2)^{tr} X} \right)^2 > 0 \quad (\text{B.41})$$

The above condition reduces to equation (27) in the text.

For part 2 of the proposition, we simply impose that  $\mu'_1 = \mu'_2$ . In this case,  $B = b_T$ ,  $A = 1$ , and (B.40) reduces to:

$$\text{var}_\psi = -X^{tr} (W'(g + \Delta g) - W'(g)) X, \quad (\text{B.42})$$

For  $\Delta g$  small,  $\text{var}_\psi > 0$  if:

$$\begin{aligned} -X^{tr} \frac{\partial W'}{\partial g} \Delta g X &> 0, \\ X^{tr} \frac{\partial W'}{\partial g} X &< 0, \\ X^{tr} \frac{\partial W'}{\partial X_2} \frac{\partial X_2}{\partial g} X &< 0, \\ X^{tr} \frac{\partial W'}{\partial X_2} X &> 0. \end{aligned} \quad (\text{B.43})$$

Using (B.25), the above condition reduces to:

$$\frac{-\rho_\epsilon (X_1 \hat{W}_A + X_2 \hat{W}_B) (X_1 W'_2 + X_2 W'_3)}{(1 + \rho_\epsilon X^{tr} W X)} > 0 \quad (\text{B.44})$$

Using equations (A.49) and (B.25), the above condition reduces to:

$$\frac{-\rho_\epsilon X^{tr} W X \hat{W}_B}{(1 + \rho_\epsilon X^{tr} W X)^2} > 0 \quad (\text{B.45})$$

Since  $X^{tr} W X > 0$  from Proposition 1, the condition reduces to  $\hat{W}_B < 0$ , which holds if and only if  $g > I_1$ .

## C Computational Details

Here we provide a short overview of the computational solution method. See Kelly and Tan (2015), Appendix B and Fitzpatrick and Kelly (2017) for full details on the solution method used here. We use a multidimensional spline approximation of the value function and value function iteration to solve the dynamic program. That is, we replace the value function on the right hand side of the Bellman equation with a spline approximation  $\hat{v}(s; p_m)$  where  $p_m$  denotes the vector of parameters of the spline at iteration  $m$ . We use Gaussian quadrature to approximate the integral in (A.40). Let  $\{b_{ij}\}_{j=1\dots J}$  denote the base points and  $\{w_{ij}\}_{j=1\dots J}$  the weights. The approximation to the Bellman's equation is then:

$$v_{m+1}(s_i) = \max_{k', \alpha, g} \left\{ \frac{c^{1-\omega}}{1-\omega} + r(t) \sum_{j=1}^J \hat{v}(s'_i(s_i, k', \alpha, g, b_{ij}); p_m) \Phi(b_{ij}, 0, 1) w_{ij} \right\}, \quad (\text{C.1})$$

subject to the model's constraints.

### C.1 Algorithm Summary

1. **Initialization.** We form a grid  $\tilde{s} = \{s_i\}_{i=1}^I$  of feasible state variables. Table A1 gives the collocation nodes that form the grid. The curse of dimensionality limits the number of grid points such that the model solves within a reasonable amount of time. Therefore, the selection of collocation nodes cannot be arbitrary. We use a relatively large number of collocation nodes for  $T$  and  $\mu$  since uncertainty over the climate sensitivity with fat tails implies that a very wide range of values for  $T$  and  $\mu$  are possible outcomes. In contrast, the range of  $W$  is small and decreases monotonically after each time period and therefore requires the fewest grid points. In addition, the value function has significant curvature in the  $k$ ,  $T$ , and  $\mu$  dimensions, which

requires additional grid points to estimate accurately. It is also important to allocate grid points near the initial condition,  $s_0$ .

2. **Spline Initialization.** We use a cubic spline approximation of the value function. The cubic spline has 3 parameters for each collocation node, except in the  $W$  dimensions, which have 2. The parameters ensure that the spline fits the value function exactly at each grid point, and that the spline is twice continuously differentiable. We choose the initial approximation parameters to fit a function satisfying known properties of the true value function such as concavity in  $k$  and decreasing in  $T$ ,  $\mu$ , and  $W$ .
3. **Maximization.** For each grid point  $s_i$ , we use  $\hat{v}(s'_i(s_i, k', \alpha, g, b_{ij}); p_m)$  to find  $\alpha$ ,  $g$ , and  $k'$  and therefore  $v_{m+1}(s_i)$  using the approximate Bellman equation (C.1).
4. **Numerical Integration.** Each numerical integration uses  $J = 5$  base points, and the upper and lower bounds of integration are set to the mean of  $z' \pm 3$  standard deviations. Note that  $z$  is a standard normal obtained by summing the three normally distributed random variables in the model and transforming the result to a standard normal, so the implied bounds for  $H'$  and therefore  $\epsilon'$ ,  $\tilde{\beta}$  and  $\tilde{\phi}$  will be different.
5. **Approximation.** The approximation parameters  $p_{m+1}$  are set to match  $v_{m+1}(s_i)$ , and maintain twice differentiability.
6. **Termination.** The algorithm stops if  $\|v_{m+1}(s_i) - v_m(s_i)\| \leq 0.001$ , otherwise we increment  $m$  by one and return to step 3.



State	Grid Points
$k$	0.46,0.7447,0.85,0.95,1.00,1.05,1.15,1.30
$T$	0.4,0.85,1.5,2,2.5,4,6,10,15
$m$	1,1.4473,2.25,3.5
$\hat{t}$	0,0.1,0.2,0.5,0.8,0.9,0.95,0.99,1
$\mu$	0.25,0.65,0.75,0.97
$\phi$	0.02,0.5,0.98
$W_1$	0,0.017
$W_3$	0,0.1
$W_2$	0,0.04
Total grid points: 248,832	

Table A1: Collocation points.  $k$ : capital stock per productivity adjusted person, further normalized so that the steady state is one.  $T_{AT}$ : atmospheric temperature in °C above preindustrial,  $m$ : greenhouse gas concentrations as a fraction of preindustrial levels.  $\hat{t}$ : equal to  $1 - \exp(-0.02t)$ , where  $t$  is years after 2015.  $\mu$ : mean of the prior distribution of the net feedback parameter (unit free).  $\phi$ : mean of the prior distribution of the SGE effectiveness.  $W_1$ : variance of the prior distribution for the net feedback parameter, unit free.  $W_3$ : variance of the prior distribution for the SGE effectiveness parameter, unit free.  $W_2$ : covariance of the prior distribution, unit free.

## C.2 Further Bounds on the State Space

The computational algorithm requires  $s'$  to remain on the grid, otherwise  $\hat{v}(s')$  must be extrapolated in an arbitrary way (without data). In particular, the elements of  $s'$  cannot fall outside the intervals given by the maximum and minimum values given in Table A1. Using the variance instead of the precision and mapping the time state into a bounded function means that  $W'$  and  $\hat{t}'$  will remain on the grid. For  $k$  and  $m$ , the minimum and maximum values in Table A1 are such that the planner optimally remains in the given interval.

However, keeping  $T'$ ,  $\phi'$ , and  $\mu'$  on the grid is less straightforward. Consider, for example, a grid point such that  $T$ ,  $\phi$ , or  $\mu$  equals its maximum value. Then evaluating  $s'$  on the right side of the distribution in the numerical integration must yield still higher values which are off the grid. For this reason, we manually impose upper bounds equal to the maximum values given in Table A1.

## D Calibration and Parameter Values

All of the parameter values, and the sources of their calibration, are listed in Tables A3 and A4. The parameters are taken from Nordhaus (2016) and Heutel et al. (2018), except as detailed below.

First, we use the calibration in Heutel et al. (2018) for SGE control costs and damage parameters. The DICE model combines damages from increased temperatures and increased CO<sub>2</sub> concentrations into a single function of temperature. Heutel et al. (2018) assume a decomposition of these damages into 80% from temperature, 10% from atmospheric CO<sub>2</sub> concentrations, and 10% from deep ocean concentrations. Since our model does not include a deep ocean concentration state, we assume that 20% of damages are due to the atmospheric concentration of CO<sub>2</sub> and 80% are due to temperature. This calibration yields the values for  $\pi_T$  and  $\pi_m$  which yields  $\hat{\pi}_m = \pi_m M_{1750}^2$ .

Next, the calibration of  $\xi_1$  uses results from Roe and Baker (2007). Assume a steady state where the carbon stock is twice preindustrial,  $m = 2$ . Then, assuming non-CO<sub>2</sub> forcing  $F_{EX}$  and SGE  $g$  are zero, in the steady-state  $\hat{F} = \xi_1 \eta$  from (A.47). Let  $[T_{AT} - T_{LO}](\infty) = 0$ , since in the steady state heat transfer between the ocean and atmosphere is in equilibrium. Then from equations (A.48), (A.50), and (A.55), the climate sensitivity, or steady-state atmospheric temperature from a doubling of CO<sub>2</sub>, is:

$$\Delta \bar{T}_{2\times} = T_{AT} = \frac{\xi_1 \eta}{1 - \bar{\beta}} \quad (\text{D.1})$$

Now Roe and Baker (2007) estimate an average feedback effect from various climate models as  $\bar{\beta} = 0.65$  and an average climate sensitivity of  $\Delta \bar{T}_{2\times} = 3.41$ . Given  $\eta = 3.6813$  from Nordhaus (2016), one can calibrate  $\xi_1$  as:

$$\xi_1 = (1 - \bar{\beta}) \frac{\Delta \bar{T}_{2\times}}{\eta} = 0.3242. \quad (\text{D.2})$$

However, this value substantially exceeds the value given in Nordhaus (2016) of  $\xi_1 = 0.1005$ . In addition, such a large value of  $\xi_1$  is inconsistent with recent temperature fluctuations in the sense that imposing  $\xi_1 = 0.3242$  causes the temperature to increase discretely in the first period (see equations A.47 and A.48). To get a more realistic estimate of  $\xi_1$ , either the mean feedback effect  $\bar{\beta}$  must be larger or the climate sensitivity assuming the mean feedback  $\Delta \bar{T}_{2\times}$  must be smaller. Following Kelly and Tan (2015), we set  $\Delta \bar{T}_{2\times} = 2.76$  which implies  $\xi_1 = 0.2624$ . Note that  $\Delta \bar{T}_{2\times}$  is the climate sensitivity when  $\beta$  is evaluated at its mean value. It is not the mean climate sensitivity,

which is actually infinite, due to the fat tail in the climate sensitivity distribution Kelly and Tan (2015).<sup>33</sup>

Notice that the net feedback parameter is uncertain but the forcing effect of CO<sub>2</sub> ( $\eta\xi_1$ ) is known with certainty. This follows the argument of Weitzman (2009) and Roe and Baker (2007) that only the feedback effects are uncertain.

For the initial uncertainty, Roe and Baker (2007) find that a normal prior distribution of  $\tilde{\beta}$  with prior mean  $\beta_0 = 0.65$  and variance  $W_{1,0} = 0.0169$  implies a climate sensitivity distribution which matches the distribution of climate sensitivities from various global circulation models (GCMs). We adopt these priors as initial conditions.

The remaining initial conditions are from Nordhaus (2016), except the prior distribution for SGE effectiveness. To calibrate the effectiveness of SGE, we use the effects of volcano explosions large enough to have climatic effects. In Table A2 we list the volcanoes we use in our calibration and the required information as presented in Driscoll et al. (2012).

Table A2: Volcanoes

Volcano	Eruption Date	SO <sub>2</sub> Mass [TgS]
Krakatau	Aug 27, 1883	44
Tarawera	Jun 10, 1886	4.5
Bandai	Jul 15, 1888	3.5
Santa Maria	Oct 24, 1902	30
Quizapu	Apr 10, 1932	3
Agung	Mar 17, 1963	20
Fuego	October 10, 1974	4
El Chichon	April 4, 1982	7
Pinatubo	June 15, 1991	20

We then collect data on Aerosol Optical Depth (AOD) from NASA. Top panel of Figure A1 shows these data.

<sup>33</sup>An alternative (Traeger, 2014; Nordhaus, 2016) is to assume an autoregressive coefficient close to one and a larger climate sensitivity. However, an OLS regression of the temperature equation yields a similar autoregressive coefficient and a relatively low climate sensitivity. The calibration thus trades off errors in short run temperature data and the long run results of complex global circulation models.

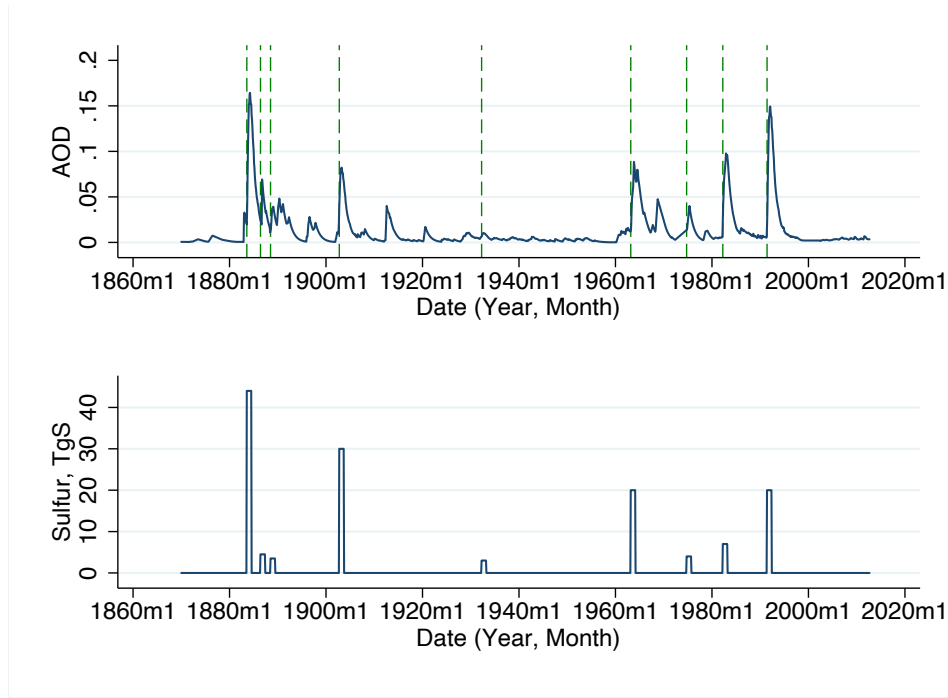


Figure A1: Sulfur and AOD

The green lines show the date of each of the volcano eruption. After each eruption there is a clear increase in AOD, which we assign the amount of sulfur associated to each volcano to the whole year following the explosion. To calculate the effect of sulfur on radiative forcing we regress:

$$AOD = \zeta_1 + \zeta_2 \text{sulfur}_t + \epsilon_t \quad (\text{D.3})$$

The result is  $\zeta_2 = 0.0027 \pm 0.00021$ . Following Ricke (2011), we assume a change of 0.1 AOD is equivalent to a reduction in radiative forcing of  $2.5 \text{ Wm}^{-2}$ . This implies based on our results that 1 TgS reduces radiative forcing by  $0.0675 \pm 0.0052 \text{ Wm}^{-2}$ . When we increase the “window of cooling” from one year to two, the results are very similar  $\zeta_2 = 0.0025 \pm .00013$ .

Finally, recall the  $g = 1$  is normalized such that 5MT sulfur causes a decrease in radiative forcing of  $\phi \eta_f$  when carbon concentrations are twice preindustrial. Since  $\zeta_2 = 0.0675$  has units of forcing per MT of sulfur, we multiply by  $5/\eta_f$  to get  $\phi = 0.0917 \pm 0.0071$ .

Our calibration suggests 20TgS (Pinatubo) are equivalent to around  $1.35 \text{ Wm}^{-2}$ . This is smaller than the usually assigned value of  $2 \text{ Wm}^{-2}$ .

Finally, we consider the calibration of the initial covariance,  $W_{2,0}$ . The covariance comes from

the passive learning model, in which  $x_{1,t}$ ,  $x_{2,t}$  and  $H_{t+1}$  are observed, generating new information to update the parameter estimates (see equations 11 and 21). However, the priors are actually formed from two different sources. The feedback prior comes from GCMs (Roe and Baker, 2007) and the effectiveness prior comes from the volcano/optical depth regressions above. One way to resolve this is to generate a prior for the covariance as if the other priors were generated from a regression using historical data on  $x_1$  and  $x_2$  via equation (11). If so, then:

$$W_0 = \rho \begin{bmatrix} \sum_{t=0}^{2015} x_{1,t}^2 & \sum_{t=0}^{2015} x_{1,t}x_{2,t} \\ \sum_{t=0}^{2015} x_{1,t}x_{2,t} & \sum_{t=0}^{2015} x_{2,t}^2 \end{bmatrix} = \rho \begin{bmatrix} 0.13^2 & W_{2,0} \\ W_{2,0} & 0.0071^2 \end{bmatrix}. \quad (\text{D.4})$$

Note that  $x_{2,t} = 0$  except for the  $m = 9$  years with volcanic eruptions noted above and  $x_{1,t}$  is the  $n = 140$  year temperature record. Under the further simplifying assumption that  $x_1$  and  $x_2$  are constant when not zero,<sup>34</sup> it follows that:

$$W_{2,0} = \sqrt{(m/n) W_{1,0} W_{3,0}} = 0.0153^2. \quad (\text{D.5})$$

Hence if  $W_{1,0}$  and  $W_{3,0}$  were generated from historical data consisting of a small number of years with volcanic eruptions and a larger number of years, without an eruption, then  $W_{2,0} = 0.0153^2$ .

Table A4 gives the exogenous variable parameters. The calibration of the exogenous variables follows Traeger (2014), updated to the 2016 version of DICE.

The emissions intensity decline rate,  $\delta_\sigma$  is calibrated to match the 2025 emissions intensity in DICE. At this value, the emissions intensity is a close match to the one in DICE for all periods. An identical procedure was used to calibrate the parameters governing the decline in the cost of the backstop technology,  $\delta_p$  and  $\theta_4$ , and the decline rate in labor productivity  $\delta_A$ . When calibrated so that backstop cost and labor productivity match the 2025 DICE values, the processes over time are a close match to DICE.

Following Traeger (2014), we assume the rate of absorption of carbon into the biosphere and deep ocean is an exogenous process given in equation (A.26), with parameters  $\delta_m(0)$ ,  $\delta_m(\infty)$ , and  $\delta_m^*$ . We choose the parameters of the absorption process so that the same DICE emissions produce similar atmospheric carbon concentrations as in the DICE model. The resulting parameters are

<sup>34</sup>This assumption can be relaxed and the result is quantitatively similar in that  $I_1$  will still be well above one and the optimal policy is largely independent of  $W_{2,0}$  in any event.

similar to Traeger (2014), except for the limiting absorption rate. In DICE, carbon is no longer absorbed after 2165 and carbon stocks fall only because sequestration is allowed at this point. To match this requires a very low limiting absorption rate.

The exogenous atmosphere-ocean temperature differential parameters  $\delta_{T,i}$ ,  $i = 1, 2, 3$ , are calibrated to match the differential in DICE. In particular, we choose the three parameters to match the initial (2015) differential, the peak differential, and so that the peak differential occurs in an identical year as in DICE.

Economic Parameters			
Parameter		Value	Source
Capital Share	$\gamma$	0.3	Nordhaus (2016)
Depreciation Rate	$\delta_k$	0.1	Nordhaus (2016)
Coefficient of Relative Risk Aversion	$\omega$	1.45	Nordhaus (2016)
Pure rate of time preference	$\delta_u$	0.015	Nordhaus (2016)
Cost and Damage Parameters			
Abatement Control Cost Exponent	$\theta_2$	2.6	Nordhaus (2016)
SGE Control Cost parameter	$\theta_{GE}$	0.0027	Heutel et. al. (2018)
SGE Control Cost exponent	$\theta_3$	2	Heutel et. al. (2018)
Temperature Damage Coefficient	$\pi_T$	0.0019	calibrated
Carbon Damage Coefficient	$\hat{\pi}_m$	0.0017	calibrated
SGE Damage Coefficient	$\pi_g$	0.03	Heutel et. al. (2018)
Climate Parameters			
Preindustrial GHG concentrations	$1/\psi$	588 GTC	Nordhaus (2016)
Radiative Forcing Parameter	$\eta$	3.6813	Nordhaus (2016)
Ocean Heat Uptake Parameter	$\xi_3$	0.088	Nordhaus (2016)
Ocean Heat Capacity	$\xi_1$	0.2624	calibrated
Initial Conditions			
Initial Capital Stock	$K_0$	\$223 Trillion	Nordhaus (2016)
Initial Carbon Stock/Preindustrial	$m_0$	1.4473	Nordhaus (2016)
Initial Temperature	$T_0$	0.85°C above 1920-40	Nordhaus (2016)
Initial mean of Prior Feedback Distribution	$\beta_0$	0.65	Roe and Baker (2007)
Initial Mean of Prior SGE Effectiveness	$\phi_0$	0.0917	calibrated
Initial Variance of Prior Feedback Distribution	$W_{1,0}$	0.13 <sup>2</sup>	Roe and Baker (2007)
Initial Variance of Prior SGE Effectiveness Distribution	$W_{3,0}$	0.0071 <sup>2</sup>	calibrated
Initial Covariance of Prior Distribution	$W_{2,0}$	0.0153 <sup>2</sup>	calibrated

Table A3: Parameter Values for endogenous equations. Values without units are unit free parameters. Units are per annum unless otherwise noted.

Economic Parameters			
Initial Population	$L(0)$	7.403B people	Nordhaus (2016)
Asymptotic Population	$L(\infty)$	11.5B people	Nordhaus (2016)
Decline Population Growth	$\delta_L$	0.0236	Nordhaus (2016)
Initial Labor Productivity	$A(0)$	10.2952 1000\$/person	Nordhaus (2016)
Initial Labor Productivity Growth	$g_A(0)$	0.0211	Nordhaus (2016)
Decline Labor Productivity Growth	$\delta_A$	0.0049	calibrated
Initial Emissions Intensity	$\sigma(0)$	0.0955 tC/1000\$	Nordhaus (2016)
Initial Emissions Intensity Growth	$g_\sigma(0)$	-0.0152	Nordhaus (2016)
Decline Emissions Intensity Growth	$\delta_\sigma$	0.001	calibrated
Initial Backstop Cost	$\theta_p$	2.0163 \$M/tC	Nordhaus (2016)
Decline Backstop Cost Growth	$\delta_p$	0.0051	calibrated
Backstop Cost Parameter	$\theta_4$	1	calibrated
Climate Parameters			
Initial Land Emissions	$E_{LAND}(0)$	0.7092 GtC	Nordhaus (2016)
Growth Rate Land Emissions	$\delta_{LAND}$	0.0223	Nordhaus (2016)
Initial Ocean Carbon Uptake	$\delta_m(0)$	0.014	calibrated
Asymptotic Ocean Uptake	$\delta_m(\infty)$	1e-6	calibrated
Decline in Ocean Carbon Uptake	$\delta_m^*$	0.016	calibrated
Initial Exogenous Forcing	$EF(0)$	0.5 $w/m^2$	Nordhaus (2016)
Asymptotic Exogenous Forcing	$EF(\infty)$	1.00 $w/m^2$	Nordhaus (2016)
Temperature Difference Parameter	$\delta_{T,1}$	0.8064	calibrated
Temperature Difference Parameter	$\delta_{T,2}$	0.0370	calibrated
Temperature Difference Parameter	$\delta_{T,3}$	-0.000176	calibrated
Variance of Weather Shocks	$\rho_\epsilon^{-1}$	0.0121	Kelly and Tan (2015)

Table A4: Parameter Values for exogenous equations. Values without units are unit free parameters. Units are per annum unless otherwise noted.

## E Learning and Forecast Errors

The rate of learning is best viewed by observing the mean absolute forecast errors over time, given the optimal decisions presented in the simulation results. For each simulation  $i$ , the forecast errors of each uncertain parameter are:

$$\text{Forecast Error}_{\beta,it} = \text{abs} \left( \tilde{\beta}_i - \beta_{it} \right), \quad (\text{E.1})$$



$$\text{Forecast Error}_{\phi,it} = \text{abs}(\tilde{\phi}_i - \phi_{it}), \quad (\text{E.2})$$

Here  $\tilde{\beta}_i$  and  $\tilde{\phi}_i$  are the true values drawn from the prior distribution for simulation  $i$ , and  $\beta_{it}$  and  $\phi_{it}$  are the means of the current beliefs each period. We similarly compute the absolute forecast errors for the climate sensitivity  $\Delta T_{2\times}$ .<sup>35</sup>

$$\text{Forecast Error}_{\Delta T_{2\times},it} = \text{abs}(\tilde{\Delta T}_{2\times,i} - \Delta T_{2\times,it}), \quad (\text{E.3})$$

Figure A2 plots the mean absolute forecast error for these three parameters.

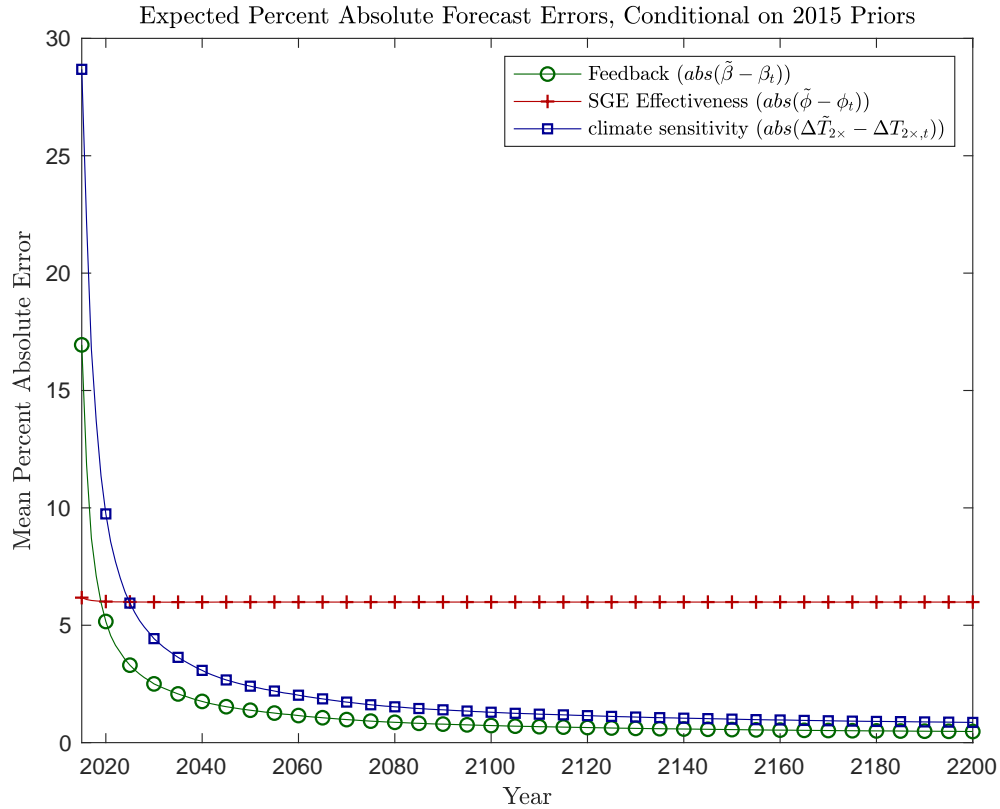


Figure A2: Mean absolute forecast errors for  $\tilde{\phi}$ ,  $\tilde{\beta}$  and  $\tilde{\Delta T}_{2\times}$ . Mean of 10,000 simulations.

The climate sensitivity distribution is fat-tailed. As shown in Kelly and Tan (2015), for most realizations of the climate sensitivity, the planner can rule out very large values quickly, reducing forecast error. However, forecast errors are difficult to reduce much beyond the initial few periods.

<sup>35</sup>Again, climate sensitivity  $\Delta T_{2\times}$  is a function of the uncertain net feedback parameter and so is itself uncertain.

Most of the remaining forecast error is driven by values of  $\tilde{\beta}$  near one (consult equation 12). Even small errors in the estimate of  $\tilde{\beta}$  generate large forecast errors in  $\Delta\tilde{T}_{2\times}$  in this case. As for SGE effectiveness, the percent forecast errors barely fall over time. The size of the SGE deployment is far too small to result in much learning. As shown in the theoretical section, SGE levels way above one are required to speed learning about SGE. Modest deployment of SGE (less than 0.1) is optimal given total costs and benefits, though it contains very little informational value.

Plotting the quantiles of forecast errors is also useful. Figure A3 plots the forecast error quantiles for the SGE effectiveness parameter  $\tilde{\phi}$ , without taking the absolute value.

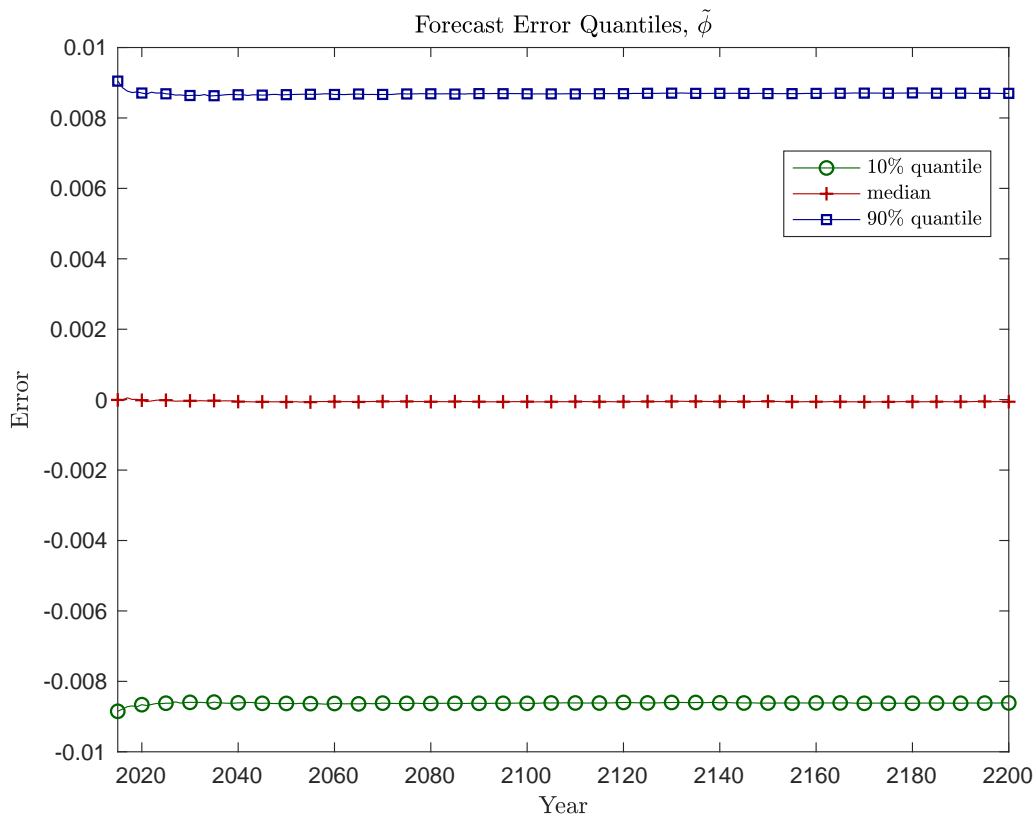


Figure A3: Forecast error quantiles for  $\tilde{\phi}$ , 10,000 simulations.

From Bayes' rule, the mean forecast errors for  $\tilde{\beta}$  and  $\tilde{\phi}$  should be zero, since Bayes' rule makes unbiased estimates. Figure A3 shows the median, which is still close to zero because the distribution for  $\tilde{\phi}$  is the symmetric normal. The 90% and 10% quantiles indicate that forecast errors remain even well past 2100 for some simulations. As a percentage of the true value, forecast errors in the lowest

10% represent average forecast errors of about -9%, whereas forecast errors in the top 10% represent average forecast errors of 10-11%.<sup>36</sup> Optimal SGE deployment is not a large enough experiment to significantly reduce these forecast errors.

Figure A4 plots the forecast error quantiles for the climate sensitivity  $\Delta\tilde{T}_{2\times}$ .

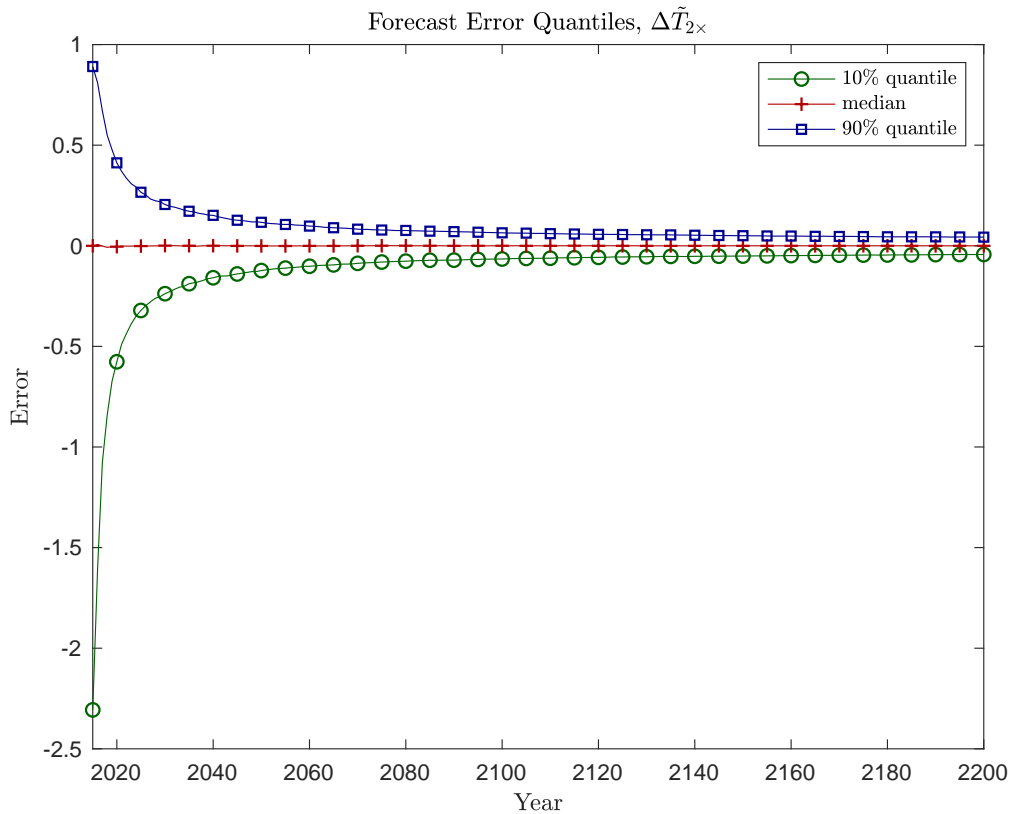


Figure A4: Forecast error quantiles for  $\Delta\tilde{T}_{2\times}$ , 10,000 simulations.

Although the error reduces to plus or minus 0.1 by 2100, learning does not improve forecasts further beyond that point, as noted above. For climate sensitivity, some learning quickly occurs initially, followed by a long period of relatively little improvement in forecast errors. Learning about both SGE effectiveness and the climate sensitivity is relatively slow, but the reasons are different. Slow learning about climate sensitivity occurs since the climate sensitivity is the weighted sum of all previous feedback effects. Thus small feedback uncertainties are magnified in the climate sensitivity. In contrast, slow learning about SGE effectiveness occurs because fast learning requires significant

<sup>36</sup>Note that the largest/smallest forecast errors result from a sequence of weather shocks in the opposite direction of the true value, not the largest/smallest true values of  $\beta$  and  $\phi$ . Therefore, the set of simulations in the top/bottom 10% in Figure A3 differ from the set of simulations in the top/bottom 10% in Figures 1-2.

use of SGE, which is not optimal.